AD-A115 566 AIR FORCE INST OF TECH WRIGHT-PATTERSON AFB OH SCHOO--ETC F/G 11/4
TIME-DOMAIN FIRST BORN APPROXIMATIONS TO ELASTODYNAMIC BACKSCAT--ETC(U)
DEC 81 G T WARHOLA
UNCLASSIFIED AFIT/GE/MA/81D-2 NL

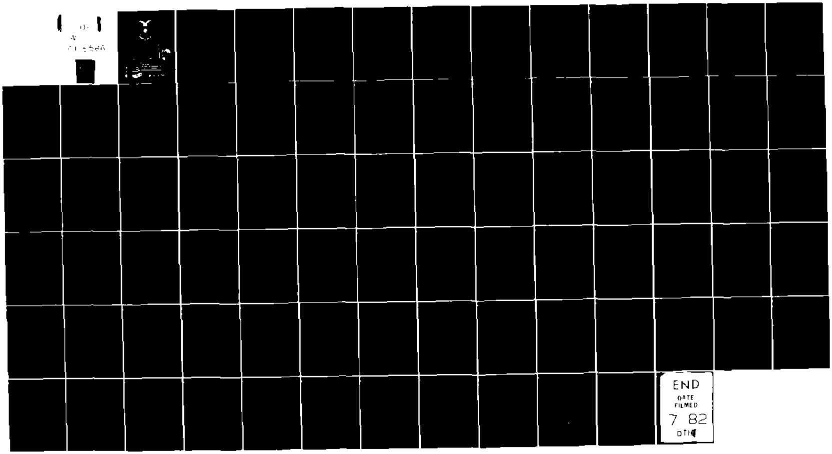

AFIT/GE/MA/81D-2

1

DTIC ELECTE JUN 15 1982

TIME-DOMAIN FIRST BORN APPROXIMATIONS
TO ELASTODYNAMIC BACKSCATTER
WITH APPLICATIONS TO NON-DESTRUCTIVE
EVALUATION OF COMPOSITES

THESIS

AFIT/GE/MA/81D-2 Gregory T. Warhola
2Lt USAF

AFIT/GE/MA/81D-2

# TIME-DOMAIN FIRST BORN APPROXIMATIONS TO ELASTODYNAMIC BACKSCATTER WITH APPLICATIONS TO NON-DESTRUCTIVE EVALUATION OF COMPOSITES

THESIS

Presented to the Faculty of the School of Engineering

of the Air Force Institute of Technology

Air University

in Partial Fulfillment of the

Requirements for the Degree of

Master of Science

| Accession For | |
|---|---|
| NTIS GRA&I | ☑ |
| DTIC TAB | ☐ |
| Unannounced | ☐ |
| Justification | |
| By | |
| Distribution/ | |
| Availability Codes | |
| Dist | Avail and/or Special |
| A | |


by

Gregory T. Warhola, B.S.

2Lt USAF

Graduate Electrical Engineering


December 1981



Approved for public release; distribution unlimited.

## Acknowledgements

I wish to express a great deal of gratitude to Dr. David A. Lee, my principal advisor, for inspiring me to undertake this project. More important than the specifics learned from this study, however, was the educational experience of interacting with the keen intellect of Dr. Lee. I thank him for the guidance he provided, his willingness to help when it was needed, and the freedom he afforded me for independent study.

Many thanks are due Dr. Robert L. Crane of the Air Force Materials Laboratory, Non-destructive Evaluation Branch (AFWAL/MLLP) for sponsoring this project and for many useful conversations regarding the non-destructive evaluation problem. I am also grateful for the computer time he made available to me.

Finally, I'd like to thank Dr. Thomas J. Moran (also at AFWAL/MLLP) for the carefully obtained experimental curves appearing in this thesis, for which I am indebted.

Gregory T. Warhola

## Contents

## List of Figures

## List of Tables

## Abstract

The first Born approximations to solutions of a time-domain integral equation were used to obtain the backscattered dilatation wave response from spherical and cylindrical inclusions of arbitrary homogeneous anisotropic elastic material embedded within a homogeneous isotropic host. For large ka, where the validity of the first Born approximation is questioned, the time waveform responses from cylinders and spheres are markedly different; for ka $\rightarrow$ 0, they have identical time form with amplitudes dependent upon the volume of the scatterer. Excellent agreement with an experimental result for scattering from a cylindrical void was obtained for a value of ka = 0.32.

A "transparency condition" was obtained, allowing that for certain combinations of both density and stiffness of the scatterer and host, the scatterer appears transparent to the incoming wave in the first Born approximation.

These results are of practical significance for non-destructive inspection of fiber-reinforced composite materials, with elastic waves of long wavelength, for determining the presence of porosity remaining in the composite after manufacturing.

# I. Introduction

## Background

Fiber-reinforced composite materials are being introduced into primary structures of modern jet fighter aircraft (e.g. vertical and horizontal stabilizers on the F-15 and F-16 fighters). These materials are made up of many layers; each layer consists of many rows of parallel fibers bound together by a matrix material of different composition than the fibers. Failure often occurs in these composites via delamination which initiates at gas bubbles (porosity) remaining in the matrix after the manufacturing process. For this and other reasons, non-destructive inspection techniques capable of determining the presence of the porosity are being sought. Current efforts include inspection with elastic waves. Items of interest include comparison of the response from the fibers to that from porosity and the degree to which the fibers may appear transparent to the waves.

For this study, the fibers are modeled as cylinders and the porosity as isolated spheres. Many studies have been done on the scattering from cylinders and isolated spheres [1-3], linear arrays of parallel cylinders [4], and two-dimensional arrays of parallel cylinders [5-6]. These studies, however, all provide frequency-domain solutions. Current inspection techniques utilize broadband time-domain pulse techniques; thus, a time-domain solution for the scattering might be more readily applied to the inspection problem.

## Problem and Scope

The problem investigated in this study is the solution for the dilatation wave backscatter from cylindrical and spherical inclusions resulting from incident dilatation pulses which are representative of the pulses produced by piezoelectric transducers. Obtaining and exploring the differences between backscatter from spheres and cylinders and comparison with an experimental result are the major objectives of this thesis. A secondary objective is a study of the transparency of common composite-reinforcing fibers to elastic waves in order to assess the feasability of non-destructive inspection with backscattered dilatation waves.

The analysis is limited to backscatter from single cylindrical or spherical inclusions of arbitrary homogeneous anisotropic elastic composition embedded in a homogeneous isotropic host. The solution for the cylinder is obtained for normal incidence of the dilatation wave with respect to the cylinder's axis of symmetry. All media are considered to obey the laws of linear elasticity and are assumed to be non-attenuative.

## Approach and Presentation

A review of Lee's development [7] of a time-domain integral equation for the scattered field is given in Chapter II, followed by a statement of the time-domain first Born approximation and the form of the solution for the scattered pulse resulting from this approximation. A "transparency condition" is then obtained for a general anisotropic homogeneous inclusion in a homogeneous isotropic host. In Chapter III, the solution for backscatter from cylinders and spheres is worked out in detail. Power series, Laplace transform methods, and recursion relations are used to obtain the solutions. Some specific results in the form of graphs of backscattered responses are presented and discussed in Chapter IV, where comparison to an experimental result is also presented. The transparency of typical fibers is also addressed in Chapter IV. Conclusions and recommendations are presented in Chapter V.

## II. Plane Pulse Scattering

The first section is intended to be a brief exposé of Lee's [7] theoretical analysis of dilatation wave backscatter from an object insonified by a plane dilatation pulse. The time-domain first Born approximation is presented therein to linearize the resulting expression for the scattered displacement field. A product of this thesis is presented in the following section where a result obtained in [7] for scattering from a void is generalized for any homogeneous anisotropic scatterer. It will be shown that, in the first Born approximation, certain combinations of density and stiffness of the host and scattering materials render the scatterer "transparent" to the incoming waves.

### The first Born approximation

Following the development of Lee [7], consider a piece R of linear elastic material bounded by the surface $\partial R$. A transducer located on a subset A of $\partial R$ launches a dilatation pulse which encounters a region B of different linear elastic material located somewhere within R, as shown in Figure 1. If B is far enough away from A, and if the radii of curvature of A are large enough compared to the dominant wavelengths of the pulse, then both the wave incident upon B and the scattered wave received by the transducer can be approximated by plane waves. The analysis which follows is

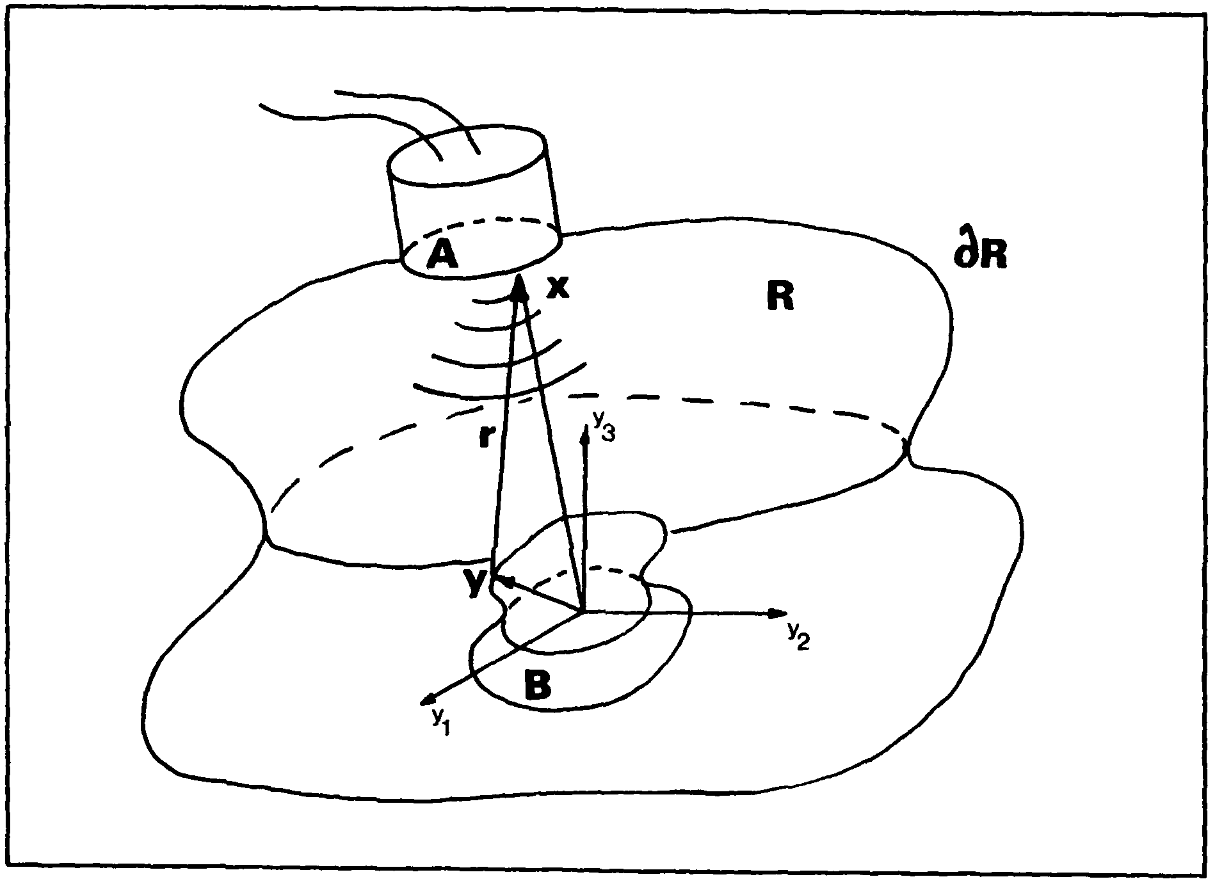


Figure 1. Scattering Configuration

not initially restricted to backscatter, i.e. the observation vector $\underline{x}$ may point in any direction. (This would, of course, require another transducer to receive the scattered waves.) The condition for backscatter is imposed later in the chapter.

The material densities and stiffness tensors are given by

$$\rho(\underline{x}) = \begin{cases} \rho^0 & , \ \underline{x} \in R-B \\ \rho^0 + \Delta\rho & , \ \underline{x} \in B \end{cases} \tag{1}$$

and

$$C_{ijkl}(\underline{x}) = \begin{cases} C^0_{ijkl} \equiv \lambda^0 \delta_{ij}\delta_{kl} + \mu^0(\delta_{ik}\delta_{jl} + \delta_{il}\delta_{jk}) , & \underline{x} \in R-B \\ C^0_{ijkl} + \Delta C_{ijkl} & , \ \underline{x} \in B \end{cases} \tag{2}$$

where $\lambda^0$ and $\mu^0$ are the Lamé constants in R-B and $\delta_{ij}$ is the Kronecker delta defined by

$$\delta_{ij} = \begin{cases} 0 & , \ i \neq j \\ 1 & , \ i = j \end{cases} \tag{3}$$

The incident pulse is of the form

$$\underline{u}^{inc}(\underline{x},t) = \nabla\phi\left[t - \frac{\underline{e}\cdot\underline{x} + \beta}{a_0}\right] \tag{4}$$

where $a_0$ is the dilatation wave speed in the region R-B and $\underline{e}$ is a unit vector characterizing the direction of propagation of the pulse. The constant $\beta$ allows the time origin to be adjusted so that $t = 0$ corresponds to the instant that the pulse first encounters B. Thus,

$$\beta = -\min(\underline{e} \cdot \underline{x}) \tag{5}$$

In (4), the scalar potential $\phi(s)$ satisfies

$$\phi(s) \in C^{(3)}(-\infty, \infty) \tag{6}$$

and

$$\phi(s) \equiv 0, \qquad s \leq 0 \tag{7}$$

A minor modification of equation (5.4.2) of reference [7] defines the pulse length $T_p$ as that time after which a specified fraction $\epsilon$ of the total energy in the pulse remains according to

$$\int_{T_p}^{\infty} |\phi(s)|^2 \, ds = \epsilon \leq 1 \tag{8}$$

The displacement field then satisfies

$$\underline{u}(\underline{x},t) = \begin{cases} \underline{u}^{inc}(\underline{x},t) &, \quad -\infty < t \leq 0 \\ \underline{u}^{inc}(\underline{x},t) + \underline{u}^{sc}(\underline{x},t) &, \quad t > 0 \end{cases} \tag{9}$$

An application of Love's integral identity [8] gives the scattered field as

$$u_i^{sc}(\underline{x},t) = \iiint_B U_{ik}\left[\underline{r}, t \,\middle|\, (\Delta c_{klmn} u^{sc}_{m,n})_{,l} - \Delta\rho \ddot{u}_k^{sc} + b_k\right] dv_y \tag{10}$$

where $b_i(x,t)$ is a body force field which is dependent upon the incident displacement field along with the density and stiffness perturbations

$$b_i(\underline{x},t) = (\Delta c_{ijkl} u^{inc}_{k,l})_{,j} - \Delta\rho \ddot{u}_i^{inc} \tag{11}$$

In (10) the dots indicate differentiation with respect to time, and the functional $U_{ik}$ is given by

$$U_{ik}[\underline{r},t\,|\,w(\cdot)] \equiv \frac{1}{4\pi\rho^{0}}\left[\frac{3r_i r_k}{r^3} - \frac{\delta_{ik}}{r}\right]\int_{1/a_0}^{1/b_0} \alpha\, w(t-\alpha r)\,d\alpha$$

$$+ \frac{r_i r_k}{r^3}\left[\frac{1}{a_0^2}\, w\left(t-\frac{r}{a_0}\right) - \frac{1}{b_0^2}\, w\left(t-\frac{r}{b_0}\right)\right]$$

$$+ \frac{\delta_{ik}}{r b_0^2}\, w\left(t-\frac{r}{b_0}\right) \tag{12}$$

where

$$r = |\underline{r}| = |\underline{x} - \underline{y}| \tag{13}$$

and $b_0$ is the shear wave speed in R-B. Equation (10) shows that the scattered field arises in an obviously nonlinear manner. It may be possible to solve for $\underline{u}^{sc}(\underline{x},t)$ by an iterative solution of (10), however, a simpler, linear problem results by assuming that the interaction of the scattered field and its derivatives with the scatterer is much smaller than that of the incident field. This requires that $\Delta c_{ijkl}$, $\Delta\rho$, $\underline{u}^{sc}(\underline{x},t)$, and $\underline{\ddot{u}}^{sc}(\underline{x},t)$ be small in some sense so that

$$\iiint_B U_{ik}\left[\underline{r},t \mid (\Delta c_{klmn} u^{sc}_{m,n})_{,l} - \Delta\rho \ddot{u}^{sc}_k\right] dv_y$$

$$<< \iiint_B U_{ik}\left[\underline{r},t \mid b_k(\underline{y},\cdot)\right] dv_y \tag{14}$$

Equation (14) is a statement of the "time-domain first Born approximation" for elastodynamic scattering which then gives the scattered field as

$$u^{sc}_i = \iiint_B U_{ik}\left[\underline{r},t \mid b_k(\underline{y},\cdot)\right] dv_y \tag{15}$$

Useful results may be obtained by considering far-field dilatation wave backscatter resulting from a plane dilatation pulse input. Generally, both dilatation and shear waves will be scattered due to mode conversion at the scatterer's boundaries; however, at distances which are large enough, time-gating may be employed to observe only the response due to the faster-traveling dilatation waves.

By expanding equation (15) with (12), discarding terms which are $O(x^{-2})$ and terms corresponding to shear waves, and applying Gauss' divergence theorem to what is left, the far-field scattered dilatation field $\hat{u}^{sc}_i(\underline{x},t)$ is obtained as

$$\hat{u}_i^{sc} = \frac{-1}{4\pi\rho^0 a_0^2 x} \iiint_B \left[ \frac{\hat{x}_i \hat{x}_k \hat{x}_l}{a_0} \Delta C_{klmn}(\underline{y}) \dot{u}^{inc}_{m,n}\left(\underline{y}, t - \frac{r}{a_0}\right) \right.$$

$$\left. + \hat{x}_i \hat{x}_k \Delta\rho(\underline{y}) \ddot{u}_k^{inc}\left(\underline{y}, t - \frac{r}{a_0}\right)\right] dv_y \qquad (16)$$

where

$$x = |\underline{x}| \qquad (17)$$

and

$$\hat{\underline{x}} = \frac{\underline{x}}{|\underline{x}|} \qquad (18)$$

Taylor's expansion of r and order of magnitude arguments allow further simplification of (16). The resulting expression for the scattered dilatation field for an incident plane dilatation pulse is

$$4\pi\rho^0 a_0^2 \hat{u}_i^{sc}(\underline{x}, t) =$$

$$-\frac{\hat{x}_i}{x} \iiint_B \left[ \frac{\hat{x}_k \hat{x}_l}{a_0^3} \Delta C_{klmn}(\underline{y}) e_m e_n + \frac{\hat{x}_k e_k}{a_0} \Delta\rho(\underline{y}) \right] \ddot{\gamma}\left(t' - \frac{\underline{e}\cdot\underline{y} + \beta}{a_0} + \frac{\hat{\underline{x}}\cdot\underline{y}}{a_0}\right) dv_y \qquad (19)$$

where

$$\Upsilon(t) \equiv \dot{\phi}(t) \tag{20}$$

is the amplitude of the incident displacement field, and

$$t' = t - \frac{x}{\alpha_0} \tag{21}$$

<u>A homogeneous anisotropic scatterer</u>

The result obtained in equation (19) is a statement of the first Born approximation for the most general anisotropic inhomogeneous scatterer embedded within an isotropic homogeneous host. Reference [7] goes on to consider further details for the special case of scattering from a void. In this thesis, equation (19) is evaluated for a homogeneous anisotropic inclusion. The solution has the same form as that for the void, with the addition of a multiplicative amplitude factor which depends upon the materials' elastic constants.

The perturbations attributable to the scatterer are taken as

$$\Delta\rho = \rho^{\beta} - \rho^{0} \tag{22}$$

and

$$\Delta c_{ijkl} = c^{B}_{ijkl} - c^{0}_{ijkl} \tag{23}$$

where $\rho^B$ and the $c^B_{ijkl}$ are constants within B, and $c^0_{ijkl}$ is as defined in equation (2). Substituting these into (19), evaluating with the Kronecker deltas, and setting $\hat{\underline{x}} = -\underline{e}$ for backscatter, yields

$$4\pi \rho^0 a_0^3 \hat{u}_i^{sc}(\underline{x},t) =$$

$$\frac{e_i}{x} \iiint_B \left\{ \left[ \rho^B - \rho^0 - \frac{\lambda^0 + 2\mu^0}{a_0^2} + \frac{e_k e_l e_m e_n c^B_{klmn}}{a_0^2} \right] \right.$$

$$\left. \times \quad \ddot{\gamma}\left(t' - \frac{2\underline{e}\cdot\underline{y} + \beta}{a_0}\right) \right\} dv_y \tag{24}$$

Consider the product $e_i e_j e_k e_l c_{ijkl}$ in (24). If the $c_{ijkl}$ are contracted according to the method described by Nye [9:131-149], the product can be written out in its full glory (for future reference) as

$$e_i e_j e_k e_l c_{ijkl} = e_1^4 c_{11} + e_2^4 c_{22} + e_3^4 c_{33}$$

$$+ 4e_2^2 e_3^2 c_{44} + 4e_1^2 e_3^2 c_{55} + 4e_1^2 e_2^2 c_{66}$$

$$+ 2e_1^2 e_2^2 c_{12} + 2e_1^2 e_3^2 c_{13} + 2e_2^2 e_3^2 c_{23}$$

$$+ 4e_1^3 e_3 c_{15} + 4e_1^3 e_2 c_{16} + 4e_1 e_2^3 c_{26}$$

$$+ 4e_2^3 e_3 c_{24} + 4e_2 e_3^3 c_{34} + 4e_1 e_3^3 c_{35}$$

$$+ 4e_1^2 e_2 e_3 c_{14} + 4e_1 e_2^2 e_3 c_{25} + 4e_1 e_2 e_3^2 c_{36}$$

$$+ 8e_1 e_2 e_3^2 c_{45} + 8e_1 e_2^2 e_3 c_{46} + 8e_1^2 e_2 e_3 c_{56} \tag{25}$$

Now, since

$$\rho^0 = \frac{\lambda^0 + 2\mu^0}{a_0^2} \tag{26}$$

and

$$C_{11}^0 = \rho^0 a_0^2 \tag{27}$$

equation (24) can be rewritten as

$$\hat{u}_i^{sc}(\underset{\sim}{x}, t) = \frac{e_i}{4\pi a_0^3 x}\left[\frac{\rho^B}{\rho^0} + \frac{e_k e_l e_m e_n C_{klmn}^B}{C_{11}^0} - 2\right]\iiint_B \ddot{\gamma}\left(t' - \frac{2\underset{\sim}{e} \cdot \underset{\sim}{y} + \beta}{a_0}\right) dv_y \tag{28}$$

Equations (25) and (28) together give the backscattered dilatation wave amplitude from any homogeneous anisotropic scatterer in the first Born approximation. This result has the same form as that obtained for a void [7], i.e., the backscattered dilatation wave amplitude is proportional to

$$\phi^{sc}(t') \equiv \iiint_B \ddot{\gamma}\left(t' - \frac{2\underline{e}\cdot\underline{y}+\beta}{a_0}\right) dv_y \tag{29}$$

It is shown in [7] that performing the integration results in

$$\phi^{sc}(t') = \frac{a_0}{2}\int_0^{t'} \ddot{\gamma}\,(t'-\tau)\,A(\tau)\,d\tau \tag{30a}$$

or

$$\phi^{sc}(t') = \frac{a_0}{2}\int_0^{t'} \gamma\,(t'-\tau)\,\ddot{A}(\tau)\,d\tau \tag{30b}$$

for both $\gamma(t) \in C^{(2)}(-\infty,\infty)$ and $A(t) \in C^{(2)}(-\infty,\infty)$, where equation (30a) is obtained for $\dot{\gamma}(0) = 0$ and (30b) for $\dot{A}(0) = 0$ . To obtain these results, a coordinate system has been introduced with the z axis parallel to $\underline{e}$ and the time $\tau$ is defined by

$$\tau = \frac{\beta + 2z}{a_0} \tag{31}$$

Note that $\tau(z_{min}) = 0$ so that

$$\beta = -2 z_{min} \tag{32}$$

The function $A(\tau)$ is a function which describes the scatterer's cross-sectional area as a function of twice the one-way transit time of the plane wave passing through the scatterer. The dependence of $A(\tau)$ upon twice the travel time makes sense physically, since the backscattered portion of a pulse which travels some distance into the scatterer must also traverse the same distance back through the scatterer.

By combining equations (28) and (29), the scattered displacement field can be expressed as

$$\hat{u}_i^{sc}(\underline{x},t) = \frac{e_i}{4\pi a_0^3 x} M \phi^{sc}(t) \tag{33}$$

where the material-dependent amplitude M is defined as

$$M \equiv \frac{\rho^B}{\rho^0} + \frac{e_k e_l e_m e_n C^B_{klmn}}{C^0_{11}} - 2 \tag{34}$$

It is instructive to consider a homogeneous isotropic inclusion B in order to obtain $M_{isotropic}$ in terms of familiar engineering quantities. It is convenient to define

$$\lambda^B \equiv \lambda^o + \Delta\lambda \tag{35}$$

$$\mu^B \equiv \mu^o + \Delta\mu \tag{36}$$

$$E^B \equiv E^o + \Delta E \tag{37}$$

$$\nu^B \equiv \nu^o + \Delta\nu \tag{38}$$

where E and $\nu$ are Young's modulus and Poisson's ratio, respectively. Substitution in (34) of an equation for $c^B_{ijkl}$, analagous to equation (2) for isotropic media, leads to

$$M_{isotropic} = \frac{\rho^B}{\rho^o} + \frac{C^B_{11}}{C^o_{11}} - 2 \tag{39}$$

Note that this expression reduces to the result obtained in [7] for scattering from a void, namely

$$M_{void} = -2 \tag{40}$$

Equation (39) is alternately expressed in terms of E and $\nu$ as

$$M_{isotropic} = \frac{\rho^B}{\rho^0} + \frac{E^B(1-\nu^B)(1+\nu^0)(1-2\nu^0)}{E^0(1-\nu^0)(1+\nu^B)(1-2\nu^B)} - 2 \tag{41}$$

which is linear in $\Delta E$ and $\Delta\nu$ .

Consider the ratio in (41)

$$R_\nu \equiv \frac{(1-\nu^B)(1+\nu^0)(1-2\nu^0)}{(1-\nu^0)(1+\nu^B)(1-2\nu^B)} \tag{42}$$

Substituting for $\nu^B$ from (38) and expanding yields

$$R_\nu = \left(\frac{1-\nu^0-\Delta\nu}{1-\nu^0}\right)\left(\frac{1}{1+\frac{\Delta\nu}{1+\nu^0}}\right)\left(\frac{1}{1-\frac{2\Delta\nu}{1-2\nu^0}}\right) \tag{43}$$

If $\Delta\nu$ satisfies

$$|\Delta\nu| \ll \begin{cases} |1+\nu^0| \quad , & -1 < \nu^0 < -1/4 \\ \left|\frac{1}{2}-\nu^0\right| \quad , & -1/4 < \nu^0 < 1/2 \end{cases} \tag{44}$$

then $R_\nu$ can be approximated by keeping the first two terms in the geometric series for the last two factors in (43)

$$R_\nu \approx 1 + \frac{2\nu^o(2-\nu^o)}{(1-{\nu^o}^2)(1-2\nu^o)}\,\Delta\nu \tag{45}$$

Thus, M is also linear in $\Delta\nu$ for small $\Delta\nu$.

The possibility of a scatterer appearing "transparent" to a plane dilatation pulse in the first *Born approximation* is suggested by equations (34) and (39). By setting M = 0, one form of the "transparency condition" for an isotropic scatterer is obtained from (41) as

$$\frac{\rho^B E^B}{\rho^o E^o} = \frac{(1-\nu^o)(1+\nu^B)(1-2\nu^B)}{(1-\nu^B)(1+\nu^o)(1-2\nu^o)}\,\frac{\rho^B}{\rho^o}\left[2-\frac{\rho^B}{\rho^o}\right] \tag{46}$$

## III. Scattering from Spheres and Cylinders

The results of the previous chapter for a scatterer of arbitrary shape are applied to spheres and cylinders. First, the cross-sectional areas of the scatterers as a function of time are determined. A model for the amplitude of an incident displacement pulse as a function of time is then introduced. The form chosen for the pulse is not only mathematically attractive, it also closely models the pulse which is produced by physical transducers. With the area and pulse functions determined, $\phi^{sc}(t)$ is evaluated according to equation (30a) for spherical and cylindrical inclusions of arbitrary isotropic linear elastic constants. The analytic character of these solutions is investigated, followed by a look at scattering in the long wavelength limit.

### Cross-sectional scattering areas

Consider a plane dilatation wave pulse traveling in the positive z direction and incident upon a spherical scatterer B, of radius s, as shown in Figure 2a. The cross-sectional area $\hat{A}_s(z)$ "seen" by the wave is the area of the family of circles subtended by the plane on the sphere

$$\hat{A}_s(z) = \begin{cases} \pi(s^2 - z^2) & , \ -s \le z \le s \\ 0 & , \ \text{otherwise} \end{cases} \tag{47}$$

Recalling equations (5) and (31) for $\beta$ and $\tau$, the area $A_s(\tau)$

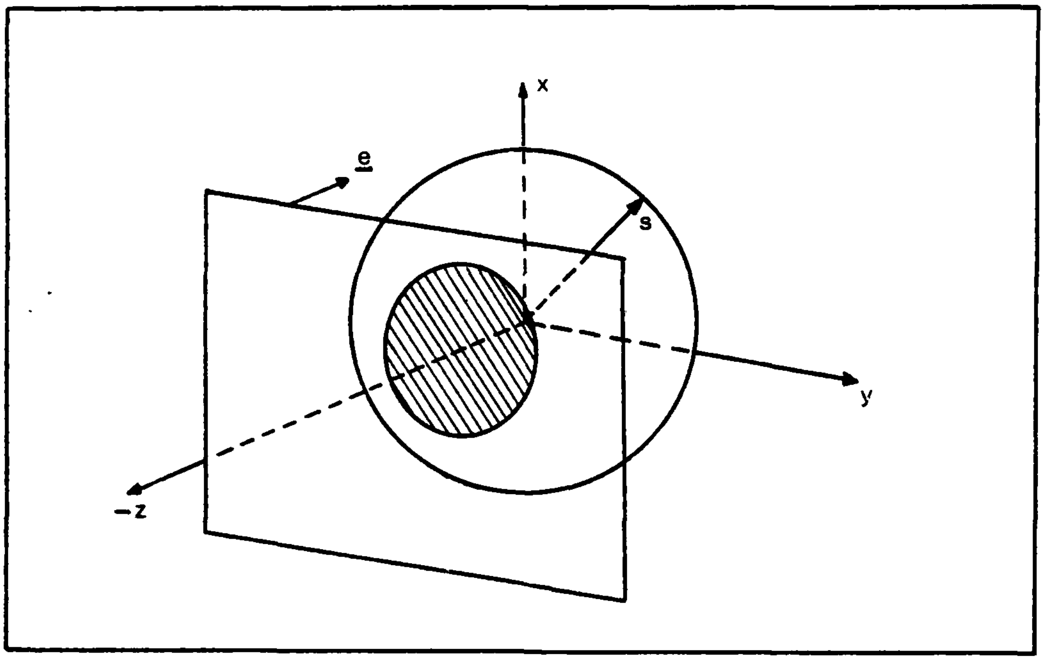


a.

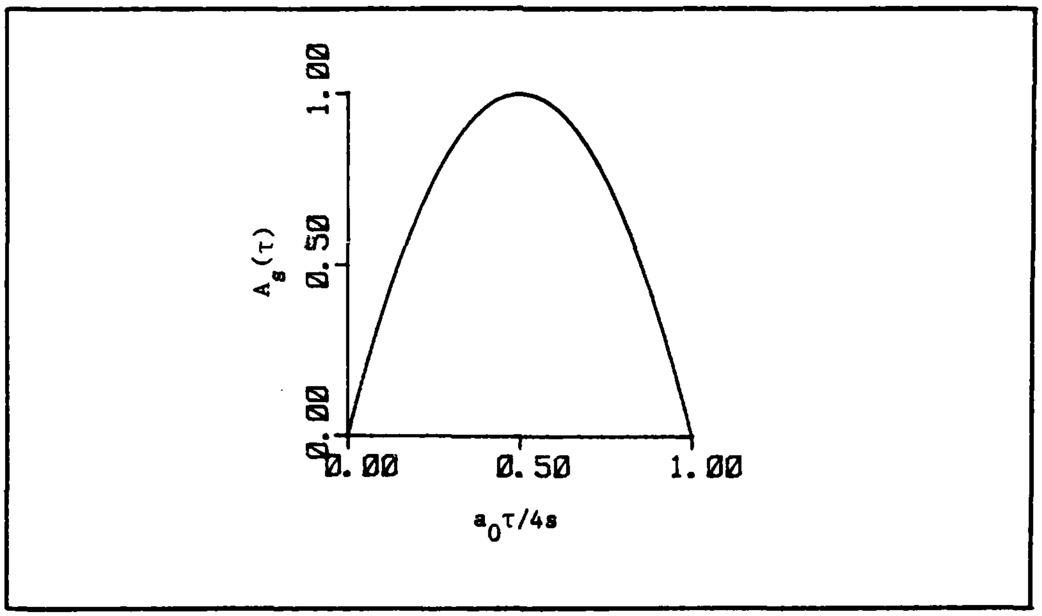


b.

Figure 2. Plane wave interaction with a sphere

is obtained as

$$A_s(\tau) = \begin{cases} \frac{\pi}{4} a_0^2 \left( \frac{4s}{a_0}\tau - \tau^2 \right) & , \; 0 \le \tau \le \frac{4s}{a_0} \\ 0 & , \; \text{otherwise} \end{cases} \tag{48}$$

$A_s(\tau)$ is parabolic as illustrated in Figure 2b.

Now, consider a dilatation wave pulse incident upon a cylinder, where the vector $\underline{e}$ is perpendicular to the axis of symmetry of the cylinder, as shown in Figure 3a. If the radius of the cylinder is c, and the length of the cylinder over which the wave can be approximated by a plane wave is L, then the cross-sectional area is the family of rectangles described by

$$\hat{A}_c(z) = \begin{cases} 2L\sqrt{c^2 - z^2} & , \; -c \le z \le c \\ 0 & , \; \text{otherwise} \end{cases} \tag{49}$$

or

$$A_c(\tau) = \begin{cases} L a_0 \sqrt{\frac{4c}{a_0}\tau - \tau^2} & , \; 0 \le \tau \le \frac{4c}{a_0} \\ 0 & , \; \text{otherwise} \end{cases} \tag{50}$$

which describes half of an ellipse, as illustrated in Figure 3b.

Since $\phi^{sc}(t)$ is given in equation (30a) as a convolution of a pulse amplitude function with $A(\tau)$, Figures 2b and

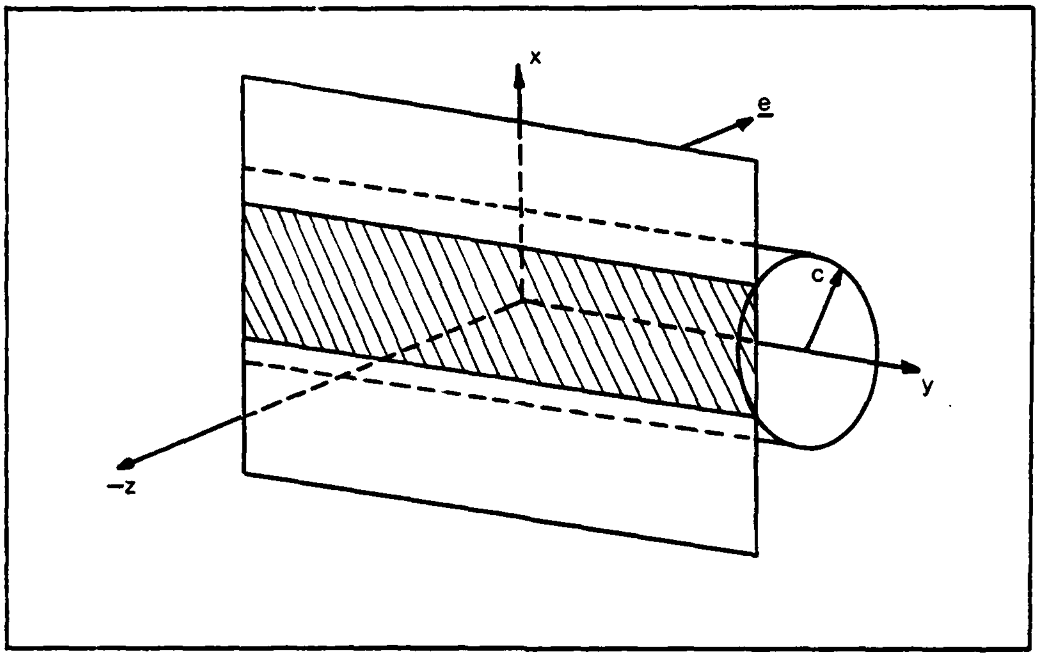


a.

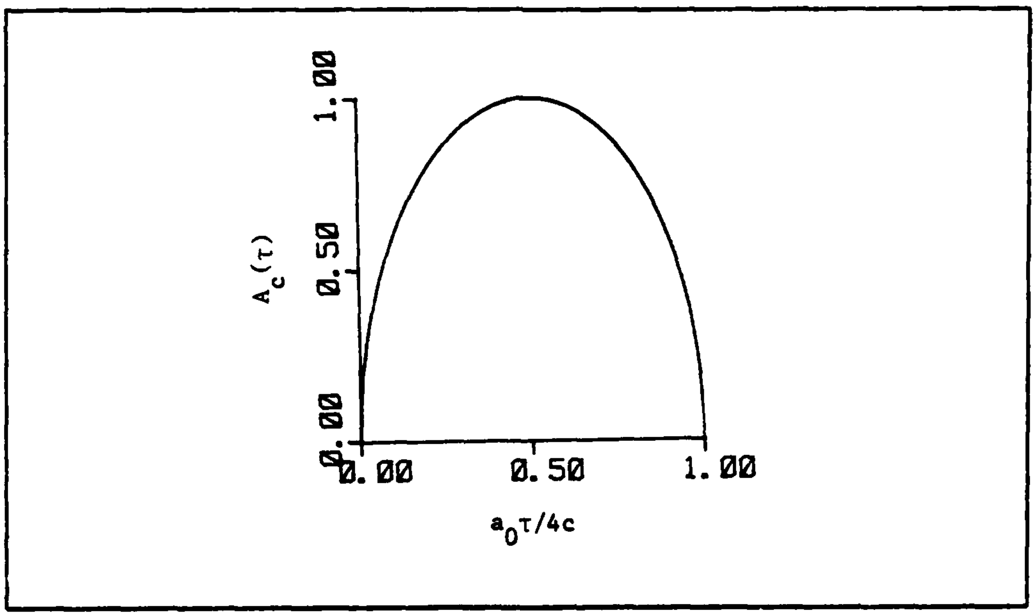


b.

Figure 3. Plane wave interaction with a cylinder

3b suggest (by considering graphical convolution) that, perhaps, spheres and cylinders will give similar scattered time waveforms. This topic is considered in the section on long wavelength scattering. However, the finite slope of the sphere's area function at $\tau = 0$ and $\tau = \frac{4s}{a_0}$ compared to the infinite slope of the cylinder's area function at the corresponding points will be shown to give characteristically different scattered responses when the long wavelength limit is not valid. Note that it is precisely the infinite slope $\dot{A}_c(0)$ which requires the use of equation (30a) instead of (30b) to obtain $\phi^{sc}(t)$ for the cylinder.

It will prove convenient, in what follows, to introduce a normalized time

$$t' = \frac{t}{2b} \tag{51}$$

where

$$b = \begin{cases} \dfrac{2s}{a_0} & \text{, sphere} \\[2ex] \dfrac{2c}{a_0} & \text{, cylinder} \end{cases} \tag{52}$$

This allows the incident pulse to be characterized in terms of the width of the scatterers' cross-sectional area time functions. Note that 2b is the time it takes the wave to completely traverse the scatterer in the incident direction and again in the backscattered direction.

Using (51) and (52) in (48) and (50), the normalized area functions are

$$\tilde{A}_s(\tau') = \begin{cases} \pi a_0^2 b^2 (\tau' - \tau'^2) & , 0 \le \tau' \le 1 \\ 0 & , \text{otherwise} \end{cases} \tag{53}$$

and

$$\tilde{A}_c(\tau') = \begin{cases} 2bLa_0 \sqrt{\tau' - \tau'^2} & , 0 \le \tau' \le 1 \\ 0 & , \text{otherwise} \end{cases} \tag{54}$$

Incident pulse model

A mathematically tractable and physically representative model of the incident plane dilatation pulse is given as

$$\gamma(t) = \begin{cases} t\, e^{-\gamma t} \sin \omega t & , t > 0 \\ 0 & , t \le 0 \end{cases} \tag{55}$$

where $\omega$ is the center frequency of the pulse. The factor of t is used to obtain $\dot{\gamma}(0) = 0$ for use of equation (30a). Differentiating twice with respect to time

$$\ddot{\gamma}(t) = \begin{cases} (g^2-\omega^2)\, t\, e^{-gt}\sin\omega t - 2g\omega t e^{-gt}\cos\omega t \\ -2g e^{-gt}\sin\omega t + 2\omega e^{-gt}\cos\omega t, & t>0 \\ \\ 0, & t\le 0 \end{cases} \tag{56}$$

Using (51) and (52) in (55) and (56), the normalized incident pulse amplitude functions are

$$\tilde{\gamma}(t') = \begin{cases} 2bt'\, e^{-2bgt'}\sin\omega' t', & t'>0 \\ 0, & t'\le 0 \end{cases} \tag{57}$$

and

$$\ddot{\tilde{\gamma}}(t') = \begin{cases} 2b(g^2-\omega^2)\, t'\, e^{-2bgt'}\sin\omega' t' - 4bg\omega t' e^{-2bgt'}\cos\omega' t' \\ -2g e^{-2bgt'}\sin\omega' t' + 2\omega e^{-2bgt'}\cos\omega' t', & t'>0 \\ \\ 0, & t'\le 0 \end{cases} \tag{58}$$

where

$$\omega' = 2b\omega \tag{59}$$

is the normalized radian frequency. In terms of the period $T = \frac{2}{\omega}\pi$,

$$T' = \frac{T}{2b} \tag{60}$$

gives the period of the pulse relative to the time width of the scatterers' area functions.

It is revealing to put this time domain pulse normalization in the perspective of the frequency domain wavenumber normalization ka employed throughout the literature, where a is the characteristic dimension of the scatterer, and $k = \frac{\omega}{a_0}$ is the wavenumber. If a corresponds to either radius, s or c, and recalling (52) and (60) for b and T',

$$ka = \frac{\pi}{2T'} \tag{61}$$

<u>Solution for the sphere</u>

With all the pieces now available, the normalized solution for the backscattered amplitude function $\tilde{\phi}_s^{sc}(t')$ for scattering from a sphere may be obtained. Either form of equation (30) may be used to obtain $\tilde{\phi}_s^{sc}(t')$ since $\dot{\tilde{A}}_s(0) = 0$.

For the form given by (30b), the required second derivative of the area function is

$$\ddot{\tilde{A}}_s(\tau') = \begin{cases} \pi a_0^2 b^2 \left[\delta(\tau') - 2 - \delta(\tau'-1)\right] & , \ 0 \leq \tau' \leq 1 \\ 0 & , \text{otherwise} \end{cases} \tag{62}$$

The delta functions greatly simplify the convolution with the incident field in (30b) and only the convolution with the constant (-2) must be worked out in detail. The situation is not so pleasant for the cylinder and equation (30a) is required due to the singular behaviour of $\dot{\tilde{A}}_c(\tau')$ at $\tau' = 0$ and at $\tau' = 1$. In order to provide a unified treatment of scattering from both objects, the form of (30a) is chosen, obtaining the solution in terms of the area function convolved with second derivative of the incident pulse.

Substituting equations (53) and (58) into (30a) produces

$$\begin{aligned} \tilde{\phi}_s^{sc}(t') = 2\pi a_0^3 b^3 \int_0^\infty \Big\{ & b(g^2-\omega^2)(t'-\tau')e^{-2bg(t'-\tau')}\sin\omega'(t'-\tau') \\ & -2bg\omega(t'-\tau')e^{-2bg(t'-\tau')}\cos\omega'(t'-\tau') \\ & -g\,e^{-2bg(t'-\tau')}\sin\omega'(t'-\tau') + \omega e^{-2bg(t'-\tau')}\cos\omega'(t'-\tau')\Big\} \\ & \times \left\{\tau' - \tau'^2\right\} d\tau' \qquad , \ t' > 0 \end{aligned} \tag{63}$$

where $d\tau = 2bd\tau'$ is employed, and

$$\alpha = \begin{cases} t' & , \quad 0 \le t' \le 1 \\ 1 & , \quad t' > 1 \end{cases} \tag{64}$$

which limits the integration to that portion of the pulse which is encountered by the wave at time t'. Introducing the complex exponent

$$K^{\pm} = 2bq \pm i\omega' \tag{65}$$

and using Euler's formulae for the sine and cosine functions, equation (62) is expanded and rearranged to obtain

$$\begin{aligned} \frac{\hat{\phi}^{sc}(t')}{2\pi a_0^3 b^2} = & -i \left\{ A^*(t') - B^*(t') \right\} \int_0^{\alpha} \tau' e^{K^- \tau'} d\tau' \\ & + i \left\{ A(t') - B(t') \right\} \int_0^{\alpha} \tau' e^{K^+ \tau'} d\tau' \\ & + i \left\{ A^*(t') \left[ t' + 1 \right] - B^*(t') \right\} \int_0^{\alpha} \tau'^2 e^{K^- \tau'} d\tau' \\ & - i \left\{ A(t') \left[ t' + 1 \right] - B(t') \right\} \int_0^{\alpha} \tau'^2 e^{K^+ \tau'} d\tau' \\ & - i \; A^*(t') \int_0^{\alpha} \tau'^3 e^{K^- \tau'} d\tau' \\ & + i \; A(t') \int_0^{\alpha} \tau'^3 e^{K^+ \tau'} d\tau' \qquad , \; t' \ge 0 \end{aligned} \tag{66}$$

where

$$A(t') \equiv \left[ \frac{b^2(q^2-\omega^2)}{2} + i\, b^2 q\, \omega \right] e^{-K^+ t'} \tag{67}$$

and

$$B(t') \equiv \left[ \frac{bq}{2} + i \frac{b\omega}{2} \right] e^{-K^+ t'} \tag{68}$$

The asterisk denotes complex conjugation and $i = \sqrt{-1}$. The integrals in (66) are easily handled by defining

$$C_j(\alpha) \equiv \int_0^\alpha \tau'^j e^{K^+ \tau'} d\tau' \tag{69}$$

Integration of (69) by parts leads to the recursion relation

$$C_j(\alpha) = \frac{\alpha^j e^{K^+ \alpha}}{K^+} - \frac{j}{K^+} C_{j-1}(\alpha) \tag{70}$$

which is particularly useful, since $C_1(\alpha)$ is readily evaluated. Note also that

$$C_j^*(\alpha) = \int_0^\alpha \tau'^j e^{K^- \tau'} d\tau' \tag{71}$$

so that (66) can be rewritten as

$$
\begin{aligned}
\frac{\tilde{\phi}_s^{sc}(t')}{2\pi a_0^3 b^2} = \; & i\left[A(t')C_1(\alpha) - A^*(t')C_1^*(\alpha)\right] t' \\
& -i\left[B(t')C_1(\alpha) - B^*(t')C_1^*(\alpha)\right] \\
& -i\left[A(t')C_2(\alpha) - A^*(t')C_2^*(\alpha)\right]\left[t'+1\right] \\
& +i\left[B(t')C_2(\alpha) - B^*(t')C_2^*(\alpha)\right] \\
& +i\left[A(t')C_3(\alpha) - A^*(t')C_3^*(\alpha)\right] \qquad , \; t'>0
\end{aligned}
\tag{72}
$$

If Im(•) denotes the imaginary part of a quantity, the back-scattered wave amplitude from a sphere is finally obtained as

$$
\begin{aligned}
\frac{\tilde{\phi}_s^{sc}(t')}{2\pi a_0^3 b^2} \quad -2 \; & \Big\{ \mathrm{Im}\left[A(t')C_1(\alpha)\right] t' \\
& - \mathrm{Im}\left[B(t')C_1(\alpha)\right] \\
& - \mathrm{Im}\left[A(t')C_2(\alpha)\right]\left[t'+1\right] \\
& + \mathrm{Im}\left[B(t')C_2(\alpha)\right] \\
& + \mathrm{Im}\left[A(t')C_3(\alpha)\right] \Big\} \qquad , \; t'>0
\end{aligned}
\tag{73}
$$

where, recall, $\alpha$ equals t' or 1 according to equation (64).

While equation (73) is not particularly revealing, it is a beautifully simple result that is, together with (69) and (70), quite amenable to numerical evaluation. It is easy enough to observe from (67) through (70) and (73) that $\tilde{\phi}_s^{sc}(t')$ has the same center frequency as $\tilde{\gamma}(t')$ and falls off as $t'e^{-2bqt'}$ for large t'.

## Solution for the cylinder

By a similar development as that for the sphere, $\tilde{\phi}_c^{sc}(t')$ is obtained for the cylinder by substituting equations (54) and (58) into (30a) producing, upon rearrangement

$$\frac{\tilde{\phi}_c^{sc}(t')}{4La_o^2 b} = \left\{\left[b^2(g^2-\omega^2)t'-bg\right]\sin\omega' t' - \left[2b^2 g t'-b\right]\omega\cos\omega' t'\right\}e^{-2bgt'}$$
$$\times\int_0^{\alpha} e^{+2bg\tau'}\sqrt{\tau'-\tau'^2}\cos\omega'\tau'\,d\tau'$$
$$-\left\{\left[b^2(g^2-\omega^2)t'-bg\right]\cos\omega' t' + \left[2b^2 g t'-b\right]\omega\sin\omega' t'\right\}e^{-2bgt'}$$
$$\times\int_0^{\alpha} e^{+2bg\tau'}\sqrt{\tau'-\tau'^2}\sin\omega'\tau'\,d\tau'$$
$$-\left\{b^2(g^2-\omega^2)\sin\omega' t' - 2b^2 g\omega\cos\omega' t'\right\}e^{-2bgt'}$$
$$\times\int_0^{\alpha} e^{+2bg\tau'}\tau'\sqrt{\tau'-\tau'^2}\cos\omega'\tau'\,d\tau'$$
$$+\left\{b^2(g^2-\omega^2)\cos\omega' t' + 2b^2 g\omega\sin\omega' t'\right\}e^{-2bgt'}$$
$$\times\int_0^{\alpha} e^{+2bg\tau'}\tau'\sqrt{\tau'-\tau'^2}\sin\omega'\tau'\,d\tau' \quad , t'>0 \tag{74}$$

where, again $\alpha$ = t' or 1 according to equation (64). The integrals in (74) lead to a solution for $\tilde{\phi}_c^{sc}(t')$ which is not as straightforward as $\tilde{\phi}_s^{sc}(t')$ obtained for the sphere.

Consider the integral

$$\tilde{I}_1(t') \equiv \int_0^{t'} e^{2bq\tau'}\sqrt{\tau'}\,(1-\tau')^{1/2}\cos\omega'\tau'\,d\tau' \tag{75}$$

Expansion of the radical in a binomial series gives

$$\tilde{I}_1(t') = \int_0^{t'}\left[e^{2bq\tau'}\sqrt{\tau'}\cos\omega'\tau'\sum_{j=0}^{\infty}(-1)^j\binom{1/2}{j}\tau'^j\right]\,d\tau' \tag{76}$$

provided $0\leq t'<1$ . Now, since the series is uniformly convergent within the interval, the summation and integration may be interchanged to obtain

$$\tilde{I}_1(t') = \sum_{j=0}^{\infty}(-1)^j\binom{1/2}{j}\Lambda_j^c(t') \tag{77}$$

where

$$\Lambda_j^c(t') \equiv \int_0^{t'}\tau'^{1/2+j}\,e^{2bq\tau'}\cos\omega'\tau'\,d\tau' \tag{78}$$

Similarly,

$$\tilde{I}_2(t') \equiv \int_0^{t'} e^{2bq\tau'}\sqrt{\tau'}\,(1-\tau')^{1/2}\sin\omega'\tau'\,d\tau' \tag{79}$$

becomes

$$\tilde{I}_2(t') = \sum_{j=0}^{\infty} (-1)^j \binom{1/2}{j} \Lambda_j^s(t') \tag{80}$$

where

$$\Lambda_j^s(t') \equiv \int_0^{t'} \tau'^{\,1/2+j}\, e^{2bq\tau'} \sin\omega'\tau'\, d\tau' \tag{81}$$

The functions $\Lambda_j^c(t')$ and $\Lambda_j^s(t')$ lend themselves to recursion relations which make them computationally attractive. Integrating (78) and (81) by parts yields

$$\Lambda_j^c(t') = \frac{t'^{\,1/2+j}\, e^{2bqt'}}{(2bq)^2 + \omega'^2}\left[2bq\cos\omega't' + \omega'\sin\omega't'\right]$$

$$- \frac{\left(\frac{1}{2}+j\right)2bq}{(2bq)^2 + \omega'^2}\Lambda_{j-1}^c(t') - \frac{\frac{1}{2}+j}{(2bq)^2 + \omega'^2}\Lambda_{j-1}^s(t') \tag{82a}$$

and

$$\Lambda_j^s(t') = \frac{t'^{\,1/2+j}\, e^{2bqt'}}{(2bq)^2 + \omega'^2}\left[2bq\sin\omega't' - \omega'\cos\omega't'\right]$$

$$- \frac{\left(\frac{1}{2}+j\right)2bq}{(2bq)^2 + \omega'^2}\Lambda_{j-1}^s(t') - \frac{\frac{1}{2}+j}{(2bq)^2 + \omega'^2}\Lambda_{j-1}^c(t') \tag{82b}$$

The appearance of the recursion index j in the numerators of the forward recursion relations (82) is not desirable since truncation errors introduced in the numerical evaluation of the functions will be amplified as j gets large. A numerically stable evaluation scheme results from manipulation of (82) which leads to the reverse recursion relations

$$\Lambda_j^c(t') = \frac{1}{\frac{3}{2}+j}\left[t'^{\,3/2+j} e^{2b\gamma t'} \cos\omega' t' + \omega' \Lambda_{j+1}^s(t') - 2b\gamma \Lambda_{j+1}^c(t')\right] \qquad (83a)$$

$$\Lambda_j^s(t') = \frac{1}{\frac{3}{2}+j}\left[t'^{\,3/2+j} e^{2b\gamma t'} \sin\omega' t' + \omega' \Lambda_{j+1}^c(t') - 2b\gamma \Lambda_{j+1}^s(t')\right] \qquad (83b)$$

Note that

$$\lim_{j\to\infty} \Lambda_j^c(t') = \lim_{j\to\infty} \Lambda_j^s(t') = 0 \qquad (84)$$

which is easily seen by considering (78) and (81) remembering that $0 \le t' < 1$.

Because of (84), the reverse recursion relations are also convenient in that an exact expression is not needed for one of the recurring functions in order to start the recursion. For large j,

$$\Lambda_j \approx \Lambda_{j-1} \quad , \quad j \to \infty \qquad (85)$$

So, by substituting $\Lambda_{j-1}(t')$ for $\Lambda_j(t')$ in (82), the recursion relations are started for $j \rightarrow \infty$ by

$$\Lambda_j^s \approx \frac{t'^{3/2+j} e^{2bqt'}\left[\left(\frac{3}{2}+j+2bq\right)\sin\omega' t' - \omega' \cos\omega' t'\right]}{\left(\frac{3}{2}+j+2bq\right)^2 + \omega'^2} \quad , \quad j \rightarrow \infty \tag{86a}$$

and

$$\Lambda_j^c \approx \frac{t'^{3/2+j} e^{2bqt'} \cos\omega' t' + \omega' \Lambda_j^s(t')}{3/2 + j + 2bq} \quad , \quad j \rightarrow \infty \tag{86b}$$

It would be nice to, somehow, insure that the functions are being generated correctly as j is decreased from its starting value to zero. A great deal of confidence could be placed in the scheme if the final recursions to $\Lambda_0^s(t')$ and $\Lambda_0^c(t')$ matched a known "correct" answer to within some desired degree of accuracy. Surprisingly enough, the zeroth integrals can be evaluated in closed form. This requires a momentary diversion to consider the integral

$$I \equiv \int_0^t e^{ks} s^{1/2} ds \tag{87}$$

Making the substitution $s = u^2$

$$I = 2 \int_0^{\sqrt{t}} u^2 e^{ku^2} du \tag{88}$$

which can be written as

$$I = \frac{d}{dk}\left[2\int_0^{\sqrt{t}} e^{ku^2}\,du\right] \tag{89}$$

Now, let $v^2 = ku^2$. This gives

$$I = \frac{d}{dk}\left[\frac{2}{\sqrt{k}}\int_0^{\sqrt{kt}} e^{v^2}\,dv\right] \tag{90}$$

Furthermore, the substitution $v = i\eta$, where $i = \sqrt{-1}$, renders

$$I = \frac{d}{dk}\left[\frac{2i}{\sqrt{kt}}\int_0^{-i\sqrt{kt}} e^{-\eta^2}\,d\eta\right] \tag{91}$$

which is recognized to contain a form [10:297] of the complex error function

$$I = \frac{d}{dk}\left[-i\sqrt{\frac{\pi}{k}}\,\mathrm{erf}\left(i\sqrt{kt}\right)\right] \tag{92}$$

Performing the indicated differentiation [10:298]

$$I = \frac{\sqrt{t}}{k}e^{kt} + i\sqrt{\frac{\pi}{4k^3}}\,\mathrm{erf}\left(i\sqrt{kt}\right) \tag{93}$$

Back to evaluating $\Lambda_0^s(t')$ and $\Lambda_0^c(t')$, Euler's formulae for the sine and cosine functions in (78) and (81), and an application of (93) to both yield

$$\Lambda_0^c(t') = \frac{\sqrt{t'}\, e^{2bqt'}}{(2bq)^2 + \omega'^2} \left[ 2bq \cos\omega' t' + \omega \sin\omega' t' \right]$$

$$+ i \frac{\sqrt{\pi}}{4} \left[ \frac{\operatorname{erf}(i\sqrt{K^+ t'})}{(K^+)^{3/2}} - \frac{\operatorname{erf}(i\sqrt{K^- t'})}{(K^-)^{3/2}} \right] \tag{94a}$$

and

$$\Lambda_0^s(t') = \frac{\sqrt{t'}\, e^{2bqt'}}{(2bq)^2 + \omega'^2} \left[ 2bq \sin\omega' t' - \omega \cos\omega' t' \right]$$

$$+ \frac{\sqrt{\pi}}{4} \left[ \frac{\operatorname{erf}(i\sqrt{K^+ t'})}{(K^+)^{3/2}} + \frac{\operatorname{erf}(i\sqrt{K^- t'})}{(K^-)^{3/2}} \right] \tag{94b}$$

where, as before $K^{\pm} = 2bq \pm i\omega'$. Equations (74), (78), and (81) can now be combined to give the solution valid for $0 \le t' < 1$, i.e. when the front edge of the pulse is within the scatterer. The result is

$$\frac{\tilde{\phi}_c^{sc}(t')}{4 L a_0^2 b} = e^{2bqt'} \sum_{j=0}^{\infty} (-1)^j \binom{1/2}{j} \Big[A_1(t')\Lambda_j^c(t')$$

$$- A_2(t')\Lambda_j^s(t') - A_3(t')\Lambda_{j+1}^c(t') + A_4(t')\Lambda_{j+1}^s(t')\Big] \quad (95)$$

where

$$A_1(t') = \left[b^2(q^2-\omega^2)t' - bq\right]\sin\omega' t' - \left[2b^2 q\omega t' - b\omega\right]\cos\omega' t' \quad (96a)$$

$$A_2(t') = \left[b^2(q^2-\omega^2)t' - bq\right]\cos\omega' t' + \left[2b^2 q\omega t' - b\omega\right]\sin\omega' t' \quad (96b)$$

$$A_3(t') = b^2(q^2-\omega^2)\sin\omega' t' - 2b^2 q\omega\cos\omega' t' \quad (96c)$$

$$A_4(t') = b^2(q^2-\omega^2)\cos\omega' t' + 2b^2 q\omega\sin\omega' t' \quad (96d)$$

The functions $\Lambda_j^s(t')$ and $\Lambda_j^c(t')$ are started by equation

(86), evaluated by equation (83), and compared to (94) to insure a desired degree of accuracy.

The solution for $t' \geq 1$ must still be obtained. Equation (74) for $\tilde{\phi}_c^{sc}(t')$ is equivalent to a form more indicative of the convolution operation (indicated by an asterisk), and thus, amenable to Laplace transform methods. The desired form of $\tilde{\phi}_c^{sc}(t')$ is

$$\frac{\tilde{\phi}_c^{sc}(t')}{4La_o^2 b} = b^2(g^2-\omega^2) f_1(t') - 2b^2 g\omega f_2(t') - bg f_3(t') + b\omega f_4(t') \tag{97}$$

where

$$f_1(t') = \left(t' e^{-2bgt'} \sin\omega' t'\right) * \Theta(t') \tag{98a}$$

$$f_2(t') = \left(t' e^{-2bgt'} \cos\omega' t'\right) * \Theta(t') \tag{98b}$$

$$f_3(t') = \left(e^{-2bgt'} \sin\omega' t'\right) * \Theta(t') \tag{98c}$$

$$f_4(t') = \left(e^{-2bgt'} \cos\omega' t'\right) * \Theta(t') \tag{98d}$$

and where

$$\Theta(t') = \begin{cases} \sqrt{t'-t'^2} & , 0 \le t' \le 1 \\ 0 & , \text{otherwise} \end{cases} \tag{99}$$

If L[•] denotes the one-sided Laplace transform of a quantity, the required transforms are evaluated in terms of the transform variable s as

$$L\left[t e^{-gt} \sin \omega t\right] = \frac{2\omega(s+g)}{\left[(s+g)^2+\omega^2\right]^2} \tag{100a}$$

$$L\left[t e^{-gt} \cos \omega t\right] = \frac{(s+g)^2-\omega^2}{\left[(s+g)^2+\omega^2\right]^2} \tag{100b}$$

$$L\left[e^{-gt} \sin \omega t\right] = \frac{\omega}{(s+g)^2+\omega^2} \tag{100c}$$

$$L\left[e^{-gt} \cos \omega t\right] = \frac{s+g}{(s+g)^2+\omega^2} \tag{100d}$$

and from [11:138],

$$L\left[\sqrt{t-t^2}\right] = \frac{\frac{\pi}{2} e^{-s/2} I_1(s/2)}{s} \tag{101}$$

where $I_\nu(\cdot)$ is the modified Bessel function of the first kind of order $\nu$. Denoting $L[f_i(t')]$ by $F_i(s)$, for i = 1,2,3,4, the $F_i(s)$ are obtained by the multiplication of the appropriate transforms in (100) by the transform in (101). The $f_i(t')$ are conveniently obtained by summing the residues at the poles of $e^{st'}F_i(s)$, which poles are, in all cases,

$$S_p^{\pm} = -K^{\pm} = -\left[2bq \pm i\omega'\right] \tag{102}$$

Note that $\frac{I_1(\frac{s}{2})}{s}$ is an entire function of s and, therefore, s = 0 is not a pole of the $F_i(s)$. Saving the details, the result, valid for $t' \geq 1$, is obtained as:

$$\begin{aligned} \frac{\tilde{\phi}_c^{sc}(t')}{4La_o^2 b} = \frac{\pi}{2}\Big\{ & \left[bq - b^2(q^2-\omega^2)t'\right] I_m\left[E(t')\right] \\ & + b\omega(1-2bqt')R_e\left[E(t')\right] \\ & - b^2(q^2-\omega^2) I_m\left[D(t')\right] \\ & - 2b^2q\omega\, R_e\left[D(t')\right]\Big\} \quad , t' \geq 1 \end{aligned} \tag{103}$$

where

$$D(t') \equiv e^{-K^+(t'-\frac{1}{2})}\left\{\frac{2I_1(\frac{K^+}{2})}{(K^+)^2} - \frac{1}{2K^+}\left[I_1\left(\frac{K^+}{2}\right) + I_0\left(\frac{K^+}{2}\right)\right]\right\} \tag{104}$$

and

$$E(t') \equiv e^{-K^+(t'-\frac{1}{2})} \frac{I_1\left(\frac{K^+}{2}\right)}{K^+} \tag{105}$$

and where Re( • ) denotes the real part of the quantity.

Equations (95) and (103) together give the solution for scattering from a cylinder for all t', including the critical point where the solutions are pieced together at t' = 1. Again, the form of the solutions is not particularly revealing, however, the same observations as those made for the scattering from the sphere can be made with respect to the scattered center frequency and the form of the solution for large t'.

Given the simplicity of the solution for $t' \geq 1$ compared to the solution for $0 \leq t' < 1$, one is tempted to look for a Laplace transform solution valid for all t'. However, the above inversions are valid only for $t' \geq 1$. Consider, for example, $e^{st'}F_3(s)$ in the form

$$e^{st'} F_3(s) = \frac{\omega\pi}{2} \frac{e^{(t'-\frac{1}{2})s}\, I_1(s/2)}{s(s-s_p^+)(s-s_p^-)} \tag{106}$$

The asymptotic expansion of $I_\nu(z)$ [10:377] for large z and $|\arg(z)| < \frac{\pi}{2}$ along with the fact that $I_1(z)$ is an odd function of z yields

$$I_1\left(\frac{s}{2}\right) \underset{|s|\to\infty}{\approx} \frac{-e^{-s/2}}{\sqrt{-\pi s}} \quad , \quad \frac{\pi}{2} < \arg(s) < 3\frac{\pi}{2} \tag{107}$$

Thus,

$$e^{st'}F_3(s) \underset{|s|\to\infty}{\approx} \frac{\omega\pi}{2\sqrt{-\pi s}} \frac{e^{(t'-1)s}}{s(s-s_p^+)(s-s_p^-)} \quad , \quad \frac{\pi}{2} < \arg(s) < 3\frac{\pi}{2} \tag{108}$$

Since the poles of $e^{st'}F_3(s)$ are in the left half of the complex plane, $e^{st'}F_3(s)$ is required to vanish as $|s|\to\infty$ in order to sum residues to obtain $f_3(t')$. However, for s in the left half plane (with a negative real part), $\lim_{|s|\to\infty} e^{st'}F_3(s) = \infty$, unless $t' \geq 1$, which therefore limits the Laplace transform solution to the region $t' \geq 1$.

## Smoothness of the solutions

The interaction of the incident pulse with scatterers having abrupt onset and terminating boundaries raises questions about the smoothness of the scattered waveforms. Recall, the scattered field's second time derivative must be sufficiently integrable so that equation (14) is satisfied for the first Born approximation to be valid. The solution for the cylinder is particularly suspect due to the infinite slope of the area function $\tilde{A}_c(\tau')$ presented to the wave at $\tau' = 0$ and $\tau' = 1$. Thus, $\tilde{\phi}_c^{sc}(t')$ is treated here first, in the form presented by equations (97) and (98).

By writing out the convolutions as integrals, keeping the first terms in the expansions for all factors in the integrands, and then performing the integrations, the result obtained is

$$\frac{\tilde{\phi}_c^{sc}(t')}{4La_0^2b} \approx \frac{2b\omega}{3} t'^{3/2} \quad , \quad t' \ll 1 \tag{109}$$

Thus,

$$\frac{\dot{\tilde{\phi}}_c^{sc}(t')}{4La_0^2b} \approx b\omega t'^{1/2} \quad , \quad t' \ll 1 \tag{110}$$

and

$$\frac{\ddot{\tilde{\phi}}_c^{sc}(t')}{4La_0^2b} \approx \frac{b\omega}{2} t'^{-1/2} \quad , \quad t' \ll 1 \tag{111}$$

Note that $\tilde{\phi}_c^{sc}(t')$, $\dot{\tilde{\phi}}_c^{sc}(t')$, and $\ddot{\tilde{\phi}}_c^{sc}(t')$ are all zero if $t'<0$. Thus, only $\ddot{\tilde{\phi}}_c^{sc}(t')$ is discontinuous at the onset of scattering, with an infinite discontinuity from a $t^{-1/2}$ singularity.

Recall, in the convolutions of (97), the upper limit of integration is t' for $0 \le t' < 1$. Differentiating with respect to t' according to Leibnitz' rule [12] yields

$$\frac{\dot{\tilde{\phi}}_c^{sc}(t')}{4La_o^2 b} = \begin{aligned}[t] & -2bq\left[b^2(q^2-\omega^2) - b\omega\omega'\right] f_1(t') \\ & + \left[\omega' b^2(q^2-\omega^2) + 4b^3q^2\omega\right] f_2(t') \\ & + \left[b^2(q^2-\omega^2) + 2b^2q^2 - b\omega\omega'\right] f_3(t') \\ & - \left[4b^2q\omega + bq\omega'\right] f_4(t') \\ & + b\omega\sqrt{t'-t'^2} \qquad , 0 \le t' \le 1 \end{aligned} \tag{112}$$

where the $\dot{f}_i(t')$ obviously give back combinations of the $f_i(t')$ and the last term results from differentiating $f_4(t')$ ala Leibnitz. For $t' \geq 1$,

$$\frac{\dot{\tilde{\phi}}_c^{sc}(t')}{4La_o^2 b} = -2bq\left[b^2(q^2-\omega^2) - b\omega\omega'\right] g_1(t') + \left[\omega' b^2(q^2-\omega^2) + 4b^3q^2\omega\right] g_2(t')$$

$$+ \left[b^2(q^2-\omega^2) + 2b^2q^2 - b\omega\omega'\right] g_3(t') - \left[4b^2q\omega + bq\omega'\right] g_4(t') \tag{113}$$

where the $g_i(t')$ are the same convolution integrals as the $f_i(t')$, except that the upper limit of integration is 1, instead of t'. Since $g_i(1) = f_i(1)$, for i = 1,2,3,4, comparison of (112) and (113) implies that $\dot{\phi}_c^{sc}(t')$ is continuous at $t' = 1$. Moreover, since the $f_i(t') \in C^{(1)}(-\infty,\infty)$, the important, physically expected, result that, $\tilde{\phi}_c^{sc}(t') \in C^{(1)}(-\infty,\infty)$ is obtained. Now differentiating $\dot{\tilde{\phi}}_c^{sc}(t')$ introduces a factor of $(t'-t'^2)^{-1/2}$ for $0 \leq t' < 1$ which obviously means that $\ddot{\tilde{\phi}}_c^{sc}(t')$ is not continuous at $t' = 1$. In fact,

$$\lim_{t' \to 1^-} \frac{\ddot{\tilde{\phi}}_c^{sc}(t')}{4bLa_o^2} = -\infty \tag{114}$$

Similarly, for $t'>1$

$$\left| \lim_{t' \to 1^+} \frac{\ddot{\tilde{\phi}}_c^{sc}(t')}{4bLa_0^2} \right| < \infty \tag{115}$$

Thus, $\ddot{\tilde{\phi}}_c^{sc}(t')$ has an infinite discontinuity at $t' = 1$ just as it does at $t' = 0$.

It is reasonable to question the validity of the first Born approximation in the light of these results for $\ddot{\tilde{\phi}}_c^{sc}(t')$, since this relates directly back, through equation (33), to equation (14). The approximation is not threatened, however, since the $t'^{-1/2}$ singularity is sufficiently integrable in (12) and volume-integrable to insure that (14) holds.

The same analysis applied to the sphere yields that

$$\left.\begin{aligned} \tilde{\phi}_s^{sc}(t') &\approx \frac{b\omega}{2}t'^2 \quad , \quad t' \ll 1 \\ \dot{\tilde{\phi}}_s^{sc}(t') &\approx b\omega t' \quad , \quad t' \ll 1 \\ \ddot{\tilde{\phi}}_s^{sc}(t') &\approx b\omega \quad , \quad t' \ll 1 \end{aligned}\right\} \tag{116}$$

Again, the second derivative is discontinuous at the onset of scattering although finite for the sphere. The discontinuity $b\omega$ is alternately expressed as

$$b\omega = 2ka \tag{117}$$

where ka is as mentioned in the section on the incident pulse characteristics. The second derivative is found to be discontinuous at $t' = 1$ by $-b\omega$, and more importantly, $\tilde{\phi}_s^{sc}(t') \in C^{(1)}(-\infty,\infty)$.

## Long wavelength limit

The time-domain first Born approximation can already be thought of as a long wavelength approximation in its own right. This seems reasonable since it's an approximation based upon weak interaction of the incident field with the scatterer; weak interaction is intuitively appealing for wavelengths long compared to the size of the scatterer. However, it appears that the approximation as stated in (14) could be satisfied by sufficiently small perturbations $\Delta\rho$ and $\Delta c_{ijkl}$ even in shorter (or at least resonant) wavelength regimes. This certainly is an item begging for further attention.

The long wavelength limit is stated according to $T' \gg 1$, or equivalently, $ka \ll \frac{\pi}{2}$. In this case, equation (30a) is particularly revealing since both $A_s(\tau)$ and $A_c(\tau)$ now sample the second derivative of the incident pulse over sufficiently small intervals so as to produce results similar to convolutions with a delta function. Thus, in the long wavelength regime, spheres and cylinders produce essentially identical backscattered fields which have pulse amplitudes given, very nearly, by the second derivative of the input pulse amplitude. This result is obtained independent of the shape of any small scattering object. The most significant difference between the backscattered fields, in the long wavelength limit, will be the amplitudes of the scattered fields due to the "strength" of the delta function. This strength depends upon the size of the object and is manifested, in the case of cylinders and spheres, in the volumes $L\pi c^2$ and $4\pi s^3/3$. Of course, the material dependent amplitude factor M introduced earlier plays a role in the scattered amplitude.

As an example of how the delta function strength and M affect a backscattered response, consider the problem of distinguishing the response from a long cylindrical inclusion and a spherical void in the long wavelength limit. The scattered time functions will have indistinguishably similar form, to within a minus sign attributable to M, and only the relative amplitudes may be strikingly different. The cylindrical inclusion may very well have an M which is quite small compared to that for the spherical void. However, if the length L over which the cylinder is illuminated by the approximately planar wave is large enough, the response from the weakly scattering inclusion can dwarf the response from the relatively strongly scattering void, due to the strength $L\pi c^2$ which is unbounded in L. This problem is of considerable interest to the Air Force for non-destructive inspection of fiber-reinforced composite materials, where detection of gas bubbles (porosity) in the epoxy matrix (host) is desirable. It would be nice if the cylindrical fibers were relatively transparent to the incident dilatation pulse, as compared to a spherical void, allowing the response from the porosity to stand out against a "background" of cylinders' response. Further attention is given this item in the following chapter.

## IV. Numerical Results

Some of the numerical techniques used for computer evaluation of the scattered responses from cylindrical and spherical inclusions are presented. Responses obtained for incident pulses having various normalized center frequencies ka are then presented to illustrate the differences and similarities between scattering from cylinders and spheres. An experimental result for scattering from a cylinder is presented and a comparison made to the response predicted by the theory. Finally, the transparency of the fibers in a fiber-reinforced composite material is addressed.

### Numerical techniques

Recall, the incident pulse amplitude is modeled as an exponentially damped sinusoid according to equation (55). For the following results, the length of the pulse $T_p$ defined by equation (8) was chosen to be the time after which ten percent of the energy in the pulse remains. With a desired pulse length and center frequency specified, substitution of (55) into (8) leads to a transcendental equation for the damping q which was solved, most conveniently, by the simple method of bisection, as described in [13:65].

The error function and modified Bessel functions of complex arguments were evaluated by routines based upon the forms of the functions given in [10]. Power series and continued fractions were utilized to provide at least eight significant figures. Asymptotic expansions were employed in the appropriate regions. The reverse recursion relations (83) were considered to provide accurate results if they matched the closed form expressions (94) to seven figures. Finally, 251 points were calculated for each theoretical plot displayed from here on.

<u>Time-domain backscatter waveforms</u>

A typical incident pulse and its second derivative are shown in Figure 4, illustrating the particular case when the pulse length is equal to the period. This may, of course, be specified for a pulse of any period. The specific case of scattering when $T' = 0.5$ ($ka = \pi$) is shown in Figure 5. The most interesting difference between the responses from the cylinder and sphere occur around the point $t' = 1$. It is at this time that the portion of the wave which makes the round trip through the entire scatterer is felt at the observation point where the wave first enters the scatterer. The more interestingly "structured" response from the cylinder is due to the more abrupt nature of the change in density and stiffness which the wave sees as a result of the infinite slopes of the cylinder's area function. While the first Born approximation is not guaranteed (or expected) to be valid when ka is this large, these results are interesting in that they predict marked differences in the backscatter from cylinders and spheres at shorter wavelengths. Figure 6

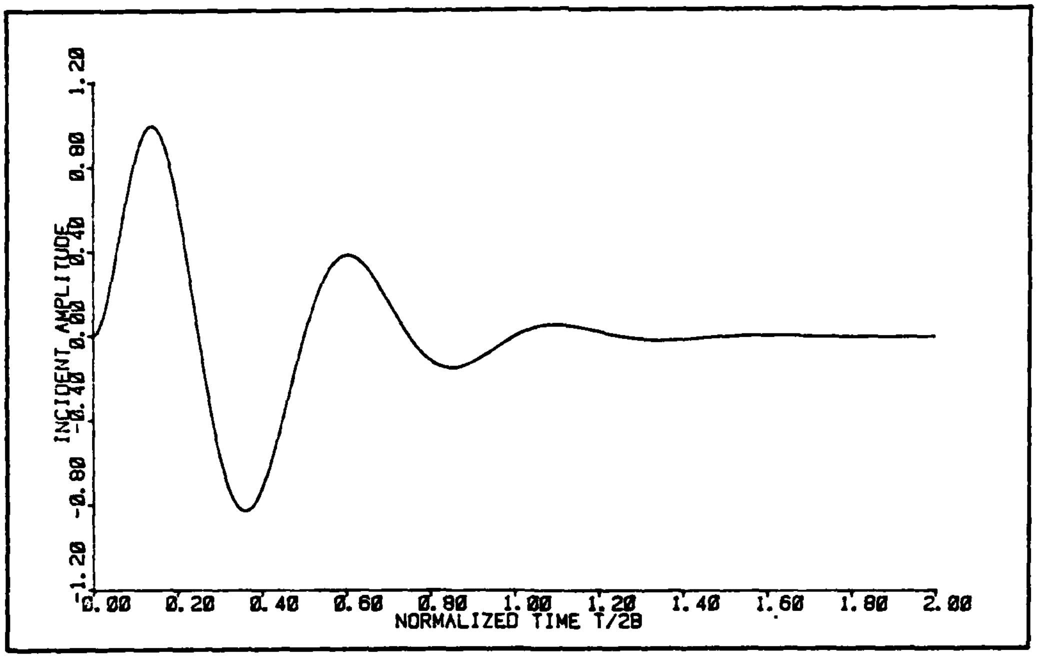


a.

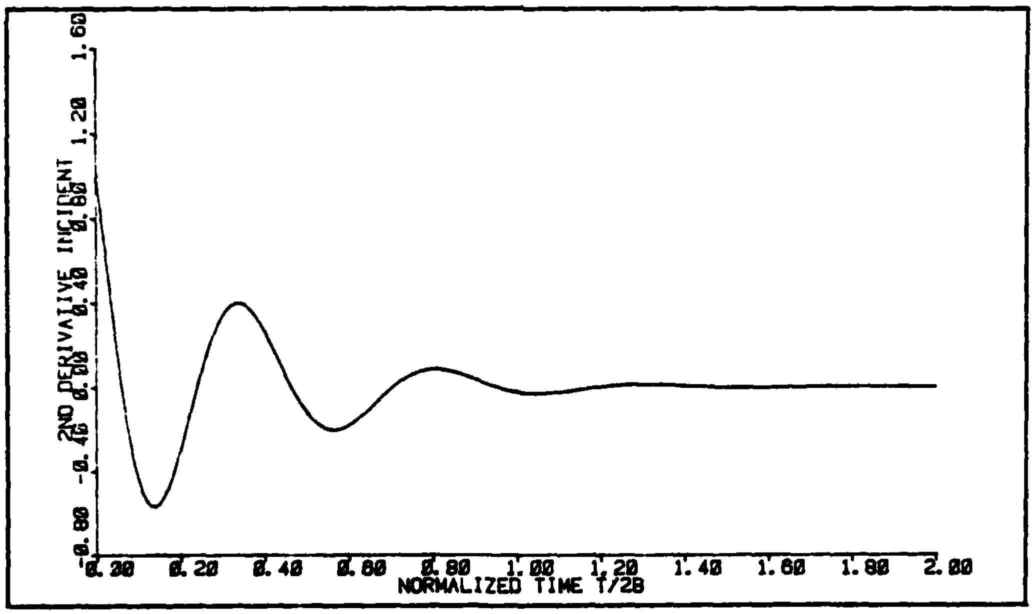


b.

Figure 4. Incident pulse waveforms

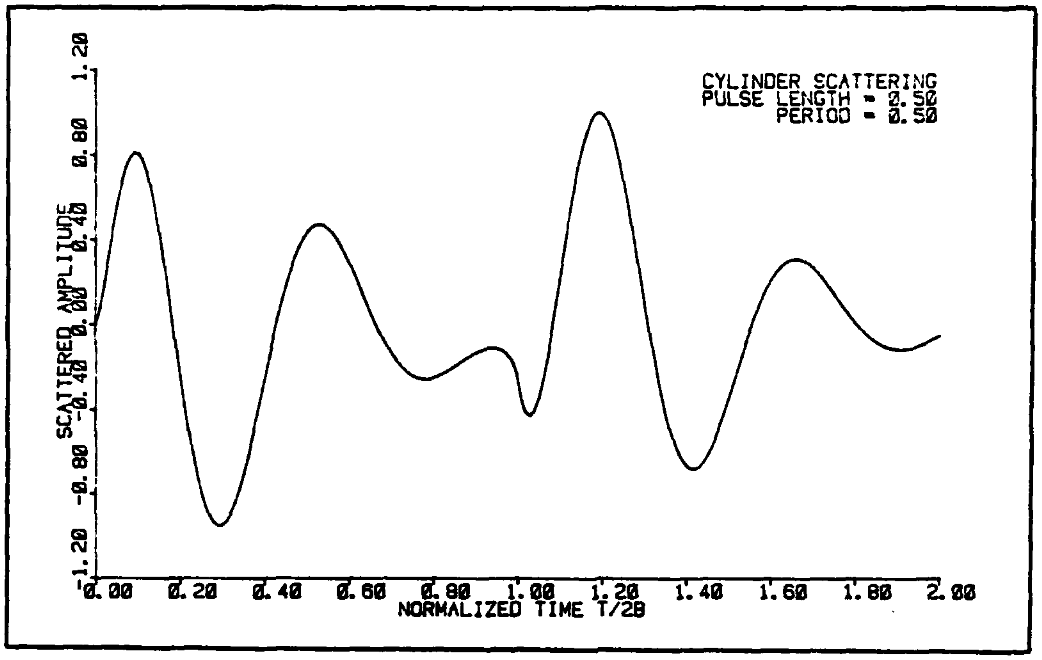


a.

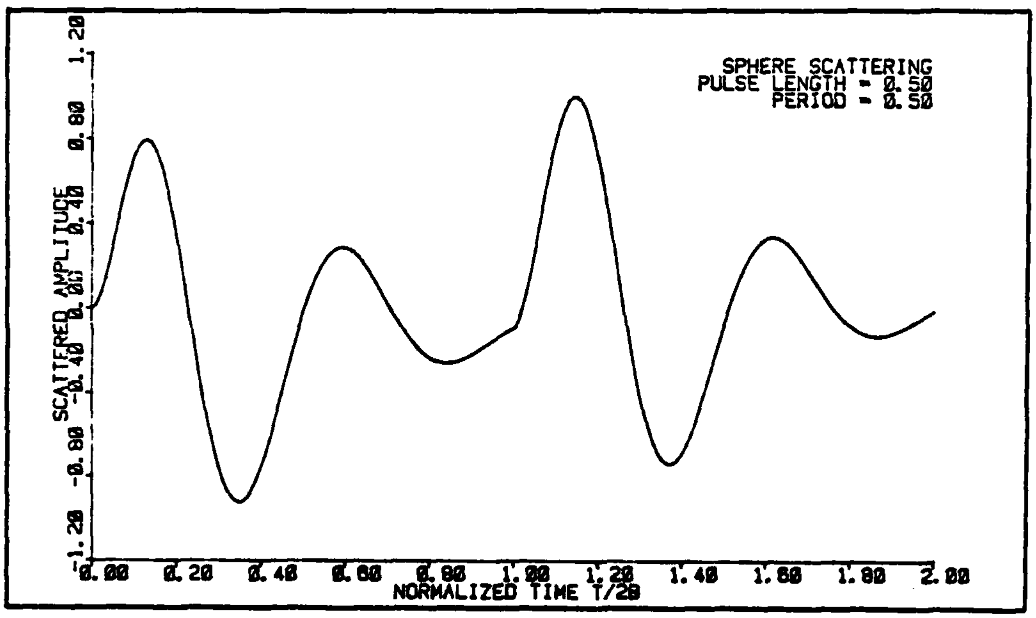


b.

**Figure 5. Backscatter for ka = π**

illustrates the scattering when $ka = \frac{\pi}{2}$, for the same pulse shape ( $T_p = T'$ ) as that in Figure 4. These results illustrate less structure around $t' = 1$ than for $ka = \pi$. This is to be expected since increasing $T_p$ and $T'$ have the effect of narrowing the bandwidth of the frequency spectrum of the incident pulse and centering it around a lower center frequency. This effect then carries through to the spectrum of the scattered pulse and is evidenced in a time-domain pulse of less structure.

## Comparison to experimental result

While the first Born approximation may be suspect for values of ka as large as in the examples above, excellent agreement between an experimental result and theoretical predictions for smaller ka will be presented.

The experiment conducted at the Air Force Materials Laboratory is illustrated in Figure 7. A voltage waveform f(t), input to the transducer, produces a plane dilatation pulse which interacts with a cylindrical void (radius 50.8 μm ) located inside a piece of linear, homogeneous, and isotropic elastic material. The scattered wave gives rise to an output voltage $g_{sc}(t)$. The incident wave also reflects from the planar "back wall" producing the response $g_{bw}(t)$. This response can be considered to be unperturbed by the incident and reflected waves traveling through the scatterer, since the magnitude of the scattered field is

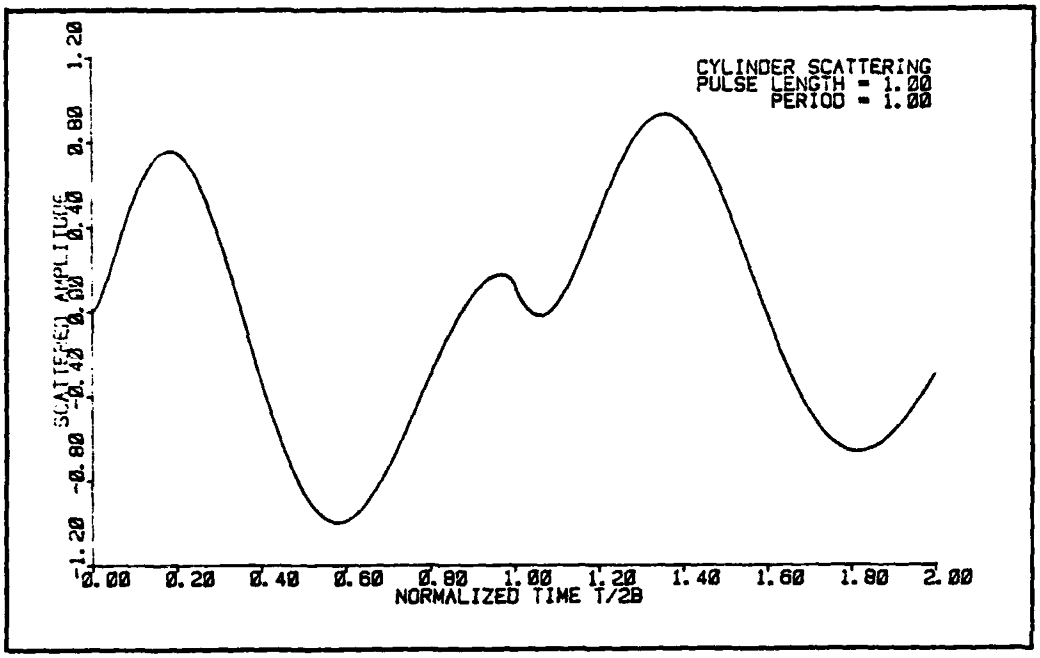


a.

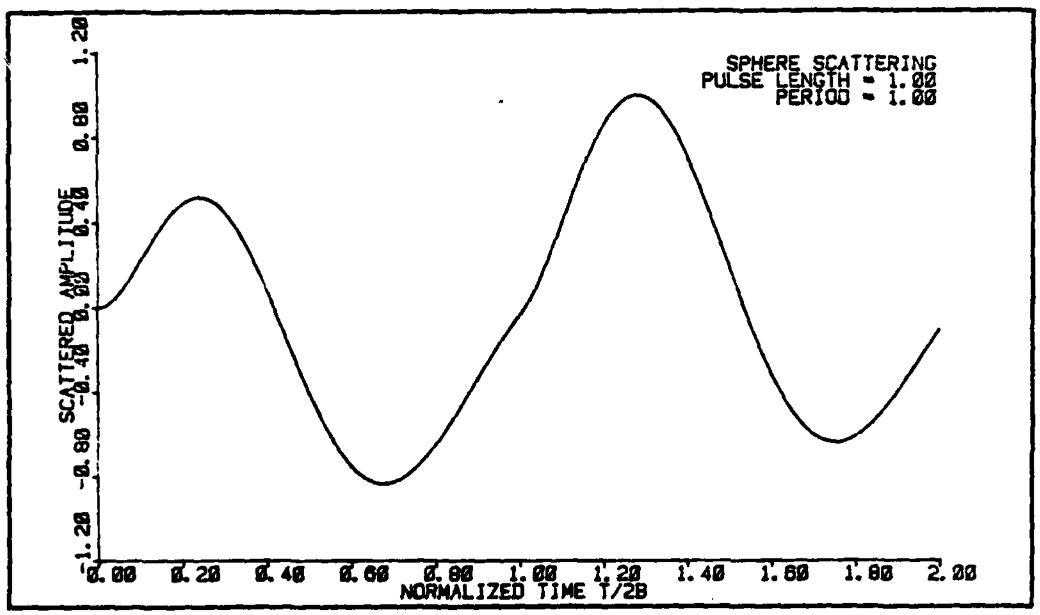


b.

Figure 6. Backscatter for ka = $\pi/2$

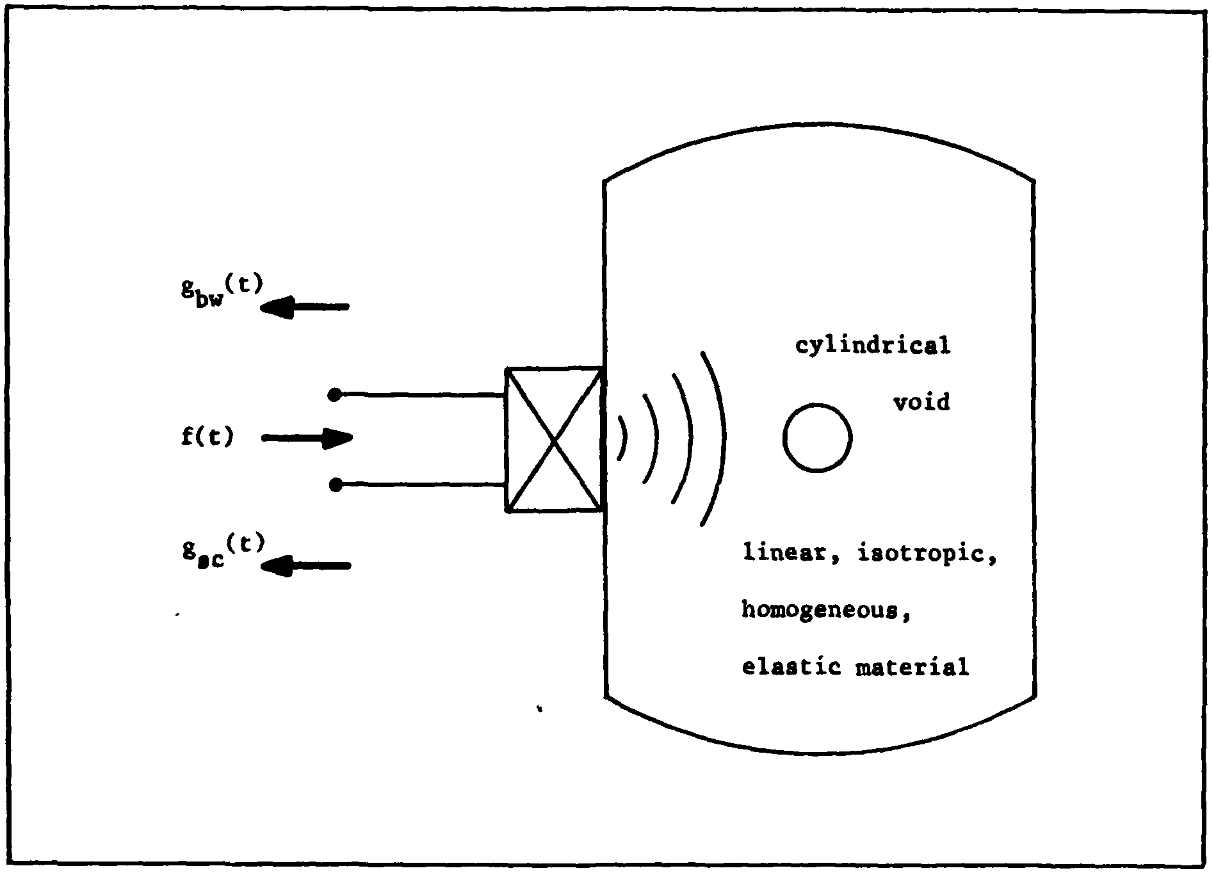


Figure 7. Scattering Experiment

much smaller than the incident and reflected fields. It is shown in [14] that treating

$$g_{sc}(t) = g_{bw}(t) * \ddot{A}(t) \tag{118}$$

is completely equivalent to treating the convolution (30a) for the scattered field.

Figure 8 shows agreement between theory and experiment for scattering from the cylindrical void when ka = 0.32 (T' = 4.85). The solid curve in Figure 8a is the back wall reflection, modeled numerically by the broken curve given by

$$\gamma(t) = t(e^{-gt} - e^{-pt})\sin\omega t \tag{119}$$

The scattered response and the numerical prediction are similarly illustrated in Figure 8b. Such agreement between theory and experiment lends credence to this approach to elastic wave scattering. The lower center frequency of the reflected pulse can be attributed to high frequency attenuation present in the host material and not accounted for in the model. The scattered pulse is not affected as much, since it travels through only about one-fourth the distance that the reflected pulse travels through. Figure 8c shows the second time derivative of equation (119). Figures b and c illustrate the result predicted earlier that the scattered field, in the long wavelength regime, is very nearly given by the second time derivative of the incident field's pulse

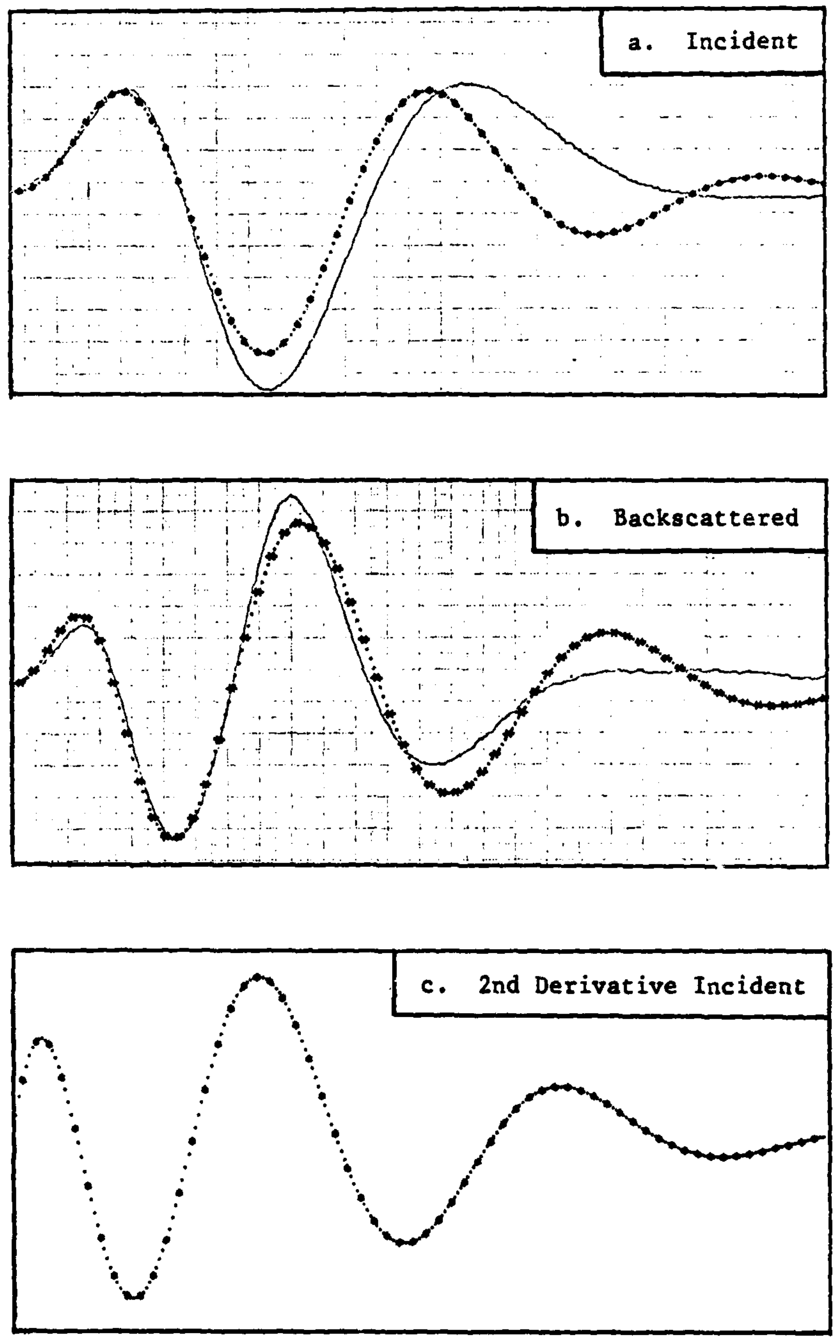


Figure 8. Comparison of an experimental result (solid line) with the theoretical prediction (broken line) for backscatter from a cylinder for ka = 0.32. The length of the abscissae is 1 μsec for all graphs.

amplitude.

Transparency considerations

The transparency of a single carbon or graphite fiber in an epoxy matrix is considered based upon the fiber elastic constants reported by Smith [15]. Adopting the notation in [15], the coordinate axes are defined with the 3 axis parallel to the fiber. For a plane dilatation pulse normally incident upon the fiber, $e_3 = 0$. Characteristics of the fiber (modeled as having hexagonal crystal symmetry) imply that $c_{16} = c_{26} = 0$, $c_{11} = c_{22}$, and $c_{66} = (c_{11} - c_{12})$. Using these to evaluate (25) for the product $e_{i'j}e_k e_l c_{ijkl}$, the amplitude $M_{fiber}$ is obtained according to (34) as

$$M_{fiber} = \frac{\rho^B}{\rho^o} + \frac{c_{11}^B}{c_{11}^o} - 2 \tag{120}$$

Note that this is the same result obtained for isotropic media in (39). This is a consequence of the hexagonal model of the fiber and the normal incidence of the dilatation pulse. It is well known [16:116] that a hexagonal structure will appear the same to a normally incident wave, independent of where $\underline{e}$ lies in the 1-2 plane, i.e., the fiber is "transversely isotropic."

Table 1 illustrates the scattering amplitudes for the fibers considered in [15].

Table I

Fiber Constants and Scattering Amplitudes

| Fiber | $\rho$ (g/cm$^3$) | $c_{11}$ ($10^{10}$ Pa) | $M_{fiber}$ | $\left(\frac{M_{fiber}}{M_{void}}\right)^2$ |
|---|---|---|---|---|
| WYB | 1.32 | 3.13 | 5.10 | 6.50 |
| T-25 | 1.38 | 1.94 | 2.89 | 2.09 |
| T-40 | 1.57 | 1.42 | 2.06 | 1.06 |
| T-50 | 1.67 | 1.25 | 1.82 | 0.83 |
| T-50S | 1.69 | 1.22 | 1.78 | 0.79 |
| T-75S | 1.88 | 0.97 | 1.47 | 0.54 |
| VYB | 1.53 | 4.92 | 8.69 | 18.88 |
| PAN | 1.72 | 2.31 | 3.88 | 3.76 |
| HTS | 1.69 | 1.60 | 2.51 | 1.58 |
| T-400 | 1.77 | 2.33 | 3.97 | 3.94 |

The epoxy density was taken as $\rho^0 = 1.16$ g/cm$^3$ and $c^0_{11}$ was calculated from $E^0 = 3.27\times10^9$ Pa and $\nu^0 = 0.35$ according to

$$c_{11} = \frac{E(1-\nu)}{(1+\nu)(1-2\nu)} \qquad (121)$$

The last column in the table compares the backscattered energy from the fibrous material to that from a void of the same shape. For only three materials is the backscattered energy less than for a void.

Practical consideration of detecting porosity in an array of fibers must also include the geometry of the scatterer, i.e., the "strength" of the scatterer mentioned in the section on long wavelength scattering. The factors $4\pi s^3/3$ and $\pi Lc^2$ are what is to be considered, not the factors $4bLa_0^2$ and $2\pi a_0^3 b^2$ appearing in equations (73), (95), and (103), which are due to the time normalization employed. Consider, for example, fibers 8 microns in diameter, illuminated by a normally incident wave which is approximately planar over a length of 1/4 inch (the size of a typical transducer face). Without considering the material parameters, the amplitude response from a single sphere will exceed that of a single fiber for porosity diameter greater than about 3.3 mils (1 mil = 25.4 microns ). By including the material-dependent amplitudes from Table 1 and requiring that $(4\pi s^3/3)M_{void}$ be greater than $\pi Lc^2 M_{fiber}$, one finds that the lower limit of porosity size that produces a larger backscattered response than an 8 micron diameter fiber varies little compared to the range of energy ratios in the table. For energy ratios varying from 0.54 to 18.88, the lower limit of "detectable" porosity varies from 3 to 5.5 mil in diameter.

# V. Conclusions and Recommendations

## Conclusions

The first Born approximations to solutions of a time-domain integral equation were used to obtain the backscattered dilatation wave response from spherical and cylindrical inclusions of arbitrary homogeneous anisotropic elastic media embedded within a homogeneous isotropic host. For relatively large values of normalized center frequency ka, the time waveform responses from cylinders and spheres are markedly different due to the difference in slopes of the scatterers' cross-sectional areas which the wave sees as it first meets the scatterer and then as it exits the scatterer. For ka $\rightarrow$ 0 the responses from the cylinder and sphere have identical time form and are given by the second derivative of the input pulse time profile; they differ in amplitude and the difference depends upon the volume of the scatterer. Excellent agreement with an experimental result for scattering from a cylindrical void was obtained at a value of ka = 0.32.

A "transparency condition" was obtained, which states that for certain combinations of both density and stiffness of the scatterer and host, the scatterer appears transparent to the incoming wave in the first Born approximation. For inclusion-host combinations which do not satisfy the condition exactly, a useful quantity is the energy scattered from an inclusion normalized to that scattered from a void. This is of practical significance for non-destructive inspection of fiber-reinforced composite materials with long wavelengths. A limitation exists on the size of spherical voids which give a larger amplitude response than a cylindrical inclusion of a given size based upon both the relative transparency of the inclusion and the volume of both scatterers illuminated by the wave. For an 8$\mu$ diameter fiber illuminated over 1/4 inch, this lower limit on the spherical void size ranges from 3 to 5.5 mil in diameter for a wide variety of fiber compositions. Since these values are within the range (1-20 mil) of practical interest, it appears from this simple analysis, that an inspection technique based solely upon backscattered waves should not be dismissed without further analysis.

Recommendations

Extensions of this study, immediately applicable to the non-destructive inspection problem, should include considerations of backscatter from spheres in the proximity of an infinite linear array of parallel cylinders. All angles of incidence with respect to the plane normal and the direction parallel to the fibers should be considered, since normal incidence alone is not usually used in current inspection techniques. Investigation of the effects of periodic, almost periodic, and random spacing of the array could prove useful. Since the number of cylinders needed to simulate the problem numerically would be very large in the long wavelength regime of interest, the computer program developed for use in this thesis would not be useful, providing as it does, complete solutions for the scattering from each fiber in the array. Further analytical work, summing the responses from the cylinders, should be carried out first, and the scattering from spheres obtained against a "background" response from the cylinders. The extension to many randomly distributed spheres near the array would then provide a model which closely approximates the physical system in the non-destructive inspection problem.

Basic questions regarding the validity of the time-domain first Born approximation need to be answered. The statement of the approximation, equation (14), suggests that perhaps, larger ka problems might be solved by this technique provided the perturbations in density and stiffness presented to the wave are sufficiently small. Certainly, as $\Delta\rho \rightarrow 0$ and $\Delta c_{ijkl} \rightarrow 0$, the backscatter goes to zero, and a regime of first Born validity should exist for small material perturbations. Another nagging point is the artificial unboundedness of the material-dependent amplitude factor M in the ratios of density and stiffness. An upper bound needs to be obtained for the magnitude of M beyond which the first Born approximation ceases to be usable.

## Bibliography


1. Faran, J. J. "Sound Scattering by Solid Cylinders and Spheres," Journal of the Acoustical Society of America, 23: 405-418 (July 1951).

2. Schuetz, L. S. and W. G. Neubauer. "Acoustic Reflection from Cylinders, Absorbing and Non-absorbing," Journal of the Acoustical Society of America, 62: 513-517 (September 1977).

3. Dragonnette, L. R. and L. Flax. "Resonance Scattering Predictions and Measurements," in Acoustic, Electromagnetic and Elastic Wave Scattering -- Focus on the T-Matrix Approach, edited by V. K. Varadan and V. V. Varadan. New York: Pergamon Press, 1980.

4. Golovchan, V. T. and A. N. Guź. "Diffraction of Elastic Waves by an Infinite Row of Circular Cylinders," Soviet Physics -- Doklady, 14-5: 503-505 (November, 1969).

5. Cheng, S. L. "Multiple Scattering of Elastic Waves by Parallel Cylinders," Journal of Applied Mechanics, 36: 523-527 (September, 1969).

6. Varadan, V. K. "Multiple Scattering of Acoustic, Electromagnetic and Elastic Waves" in Acoustic, Electromagnetic and Elastic Wave Scattering -- Focus on the T-Matrix Approach, edited by V. K. Varadan and V. V. Varadan. New York: Pergamon Press, 1980.

7. Lee, D. A. "Mathematical Principles of Data Inversion" in Non-Destructive Evaluation, edited by M. Buckley and D. Thompson. New York-Heidelberg: Springer-Verlag (in press).

8. Wheeler, L. T. and E. Sternberg. "Some Theorems in Classical Elastodynamics," Archive for Rational Mechanics and Analysis, 31: 51-90 (1968).

9. Nye, J. F. Physical Properties of Crystals. London: Oxford University Press, 1967.

10. AMS 55, Handbook of Mathematical Functions, edited by M Abramowitz and I. A. Stegun. National Bureau of Standards, 1977.

11. Bateman Manuscript Project, Volume 1, Tables of Integral Transforms, edited by A. Erdélyi. New York: McGraw-Hill, 1954.

12. Wylie, C. R. Advanced Engineering Mathematics (Fourth Edition). New York: McGraw-Hill, 1975.

13. Hornbeck, R. W. Numerical Methods. New York: Quantum, 1975.

14. Lee, D. A. "Scatter Sizing for Elastodynamic Backscattering Using Splines," Modeling and Simulation, Volume 12, Part 4, Proceedings of the Twelfth Annual Pittsburgh Conference, edited by W. G. Vogt and M. H. Mickle. 1253-1257. Pittsburgh: Instrument Society of America, 1981.

15. Smith, R. E. "Ultrasonic Elastic Constants of Carbon Fibers and Their Composites," Journal of Applied Physics, 43-6: 2555-2561 (June, 1972).

16. Auld, B. A. Acoustic Fields and Waves in Solids, Volume 1. New York: Wiley, 1973.

## Vita

Gregory T. Warhola was born on 29 April 1955 in Philadelphia, Pennsylvania. He graduated from high school in Levittown, Pennsylvania, in 1973, and attended Drexel University for a year before enlisting in the USAF, in June 1974. He was stationed at Mather AFB, California, in the 320th Bomb Wing where he performed maintenance on avionic navigational systems. He entered the Airmen Education and Commissioning Program in September 1977 and graduated with a Bachelor of Science in Electrical Engineering, at the University of Utah, in March 1980. He then received his commission at the USAF Officer Training School in June 1980 and attended the School of Engineering, Air Force Institute of Technology, in July 1980.

Permanent Address: 902 Hilary Ave.

Croydon, Pennsylvania 19020

UNCLASSIFIED

SECURITY CLASSIFICATION OF THIS PAGE (When Data Entered)

## REPORT DOCUMENTATION PAGE

READ INSTRUCTIONS BEFORE COMPLETING FORM

1. REPORT NUMBER: AFIT/GE/MA/81D-2
2. GOVT ACCESSION NO.
3. RECIPIENT'S CATALOG NUMBER
4. TITLE (and Subtitle): TIME-DOMAIN FIRST BORN APPROXIMATIONS TO ELASTODYNAMIC BACKSCATTER WITH APPLICATIONS TO NON-DESTRUCTIVE EVALUATION OF COMPOSITES
5. TYPE OF REPORT & PERIOD COVERED: MS Thesis
6. PERFORMING ORG. REPORT NUMBER
7. AUTHOR(s): Gregory T. Warhola, 2Lt USAF
8. CONTRACT OR GRANT NUMBER(s)
9. PERFORMING ORGANIZATION NAME AND ADDRESS: Air Force Institute of Technology (AFIT-EN), Wright-Patterson AFB, Ohio 45433
10. PROGRAM ELEMENT, PROJECT, TASK AREA & WORK UNIT NUMBERS
11. CONTROLLING OFFICE NAME AND ADDRESS: Air Force Materials Laboratory (AFWAL/MLLP), Wright-Patterson AFB, Ohio 45433
12. REPORT DATE: December, 1981
13. NUMBER OF PAGES: 76
14. MONITORING AGENCY NAME & ADDRESS (if different from Controlling Office)
15. SECURITY CLASS. (of this report): Unclassified
15a. DECLASSIFICATION/DOWNGRADING SCHEDULE
16. DISTRIBUTION STATEMENT (of this Report)

Approved for public release; distribution unlimited

17. DISTRIBUTION STATEMENT (of the abstract entered in Block 20, if different from Report)

15 APR 1982

Dean for Research and Professional Development
Air Force Institute of Technology (ATC)
Wright-Patterson AFB, OH 45433

18. SUPPLEMENTARY NOTES

Approved for public release; IAW AFR 190-17

~~FREDERICK C. LYNCH, Major, USAF~~
~~Director of Information~~

19. KEY WORDS (Continue on reverse side if necessary and identify by block number)

Elastodynamic Backscatter
Elastic Waves
Born Approximation
Fiber
Composite
Scatter
NDE
Non-destructive

20. ABSTRACT (Continue on reverse side if necessary and identify by block number)

The first Born approximations to solutions of a time-domain integral equation were used to obtain the backscattered dilatation wave response from spherical and cylindrical inclusions of arbitrary homogeneous anisotropic elastic material embedded within a homogeneous isotropic host. For large ka, where the validity of the first Born approximation is questioned, the time waveform responses from cylinders and spheres are markedly different; for ka $\rightarrow$ 0, they have identical time form with amplitudes dependent upon the volume of the scatterer. Excellent agreement with an experimental result for scattering from

DD FORM 1473 1 JAN 73 EDITION OF 1 NOV 65 IS OBSOLETE

UNCLASSIFIED

SECURITY CLASSIFICATION OF THIS PAGE (When Data Entered)

Block 20.

a cylindrical void was obtained for a value of $ka = 0.32$.

A "transparency condition" was obtained, allowing that for certain combinations of both density and stiffness of the scatterer and host, the scatterer appears transparent to the incoming wave in the first Born approximation.

These results are of practical significance for non-destructive inspection of fiber-reinforced composite materials, with elastic waves of long wavelength, for determining the presence of porosity remaining in the composite after manufacturing.

DATE
ILMED
8